

Disparity of turbinal bones in placental mammals

Quentin Martinez^{1,2}  | Mark Wright^{2,3} | Benjamin Dubourguier² | Kai Ito^{4,5} | Thomas van de Kamp^{6,7} | Elias Hamann⁶ | Marcus Zuber⁶ | Gabriel Ferreira^{8,9}  | Rémi Blanc¹⁰ | Pierre-Henri Fabre^{2,11,12,13} | Lionel Hautier^{2,11}  | Eli Amson¹ 

¹Staatliches Museum für Naturkunde Stuttgart, Stuttgart, Germany

²Institut des Sciences de l'Évolution (ISEM, UMR 5554 CNRS-IRD-UM), Université de Montpellier, Montpellier Cedex 5, France

³Museum of Comparative Zoology and Department of Organismic and Evolutionary Biology, Harvard University, Cambridge, Massachusetts, USA

⁴Department of Natural Environmental Studies, Graduate School of Frontier Sciences, The University of Tokyo, Chiba, Japan

⁵Department of Anatomy, School of Dental Medicine, Tsurumi University, Yokohama, Japan

⁶Institute for Photon Science and Synchrotron Radiation (IPS), Karlsruhe Institute of Technology (KIT), Eggenstein-Leopoldshafen, Germany

⁷Laboratory for Applications of Synchrotron Radiation (LAS), Karlsruhe Institute of Technology (KIT), Karlsruhe, Germany

⁸Senckenberg Centre for Human Evolution and Palaeoenvironment at the Eberhard Karls University of Tübingen, Tübingen, Germany

⁹Department of Geosciences, Faculty of Sciences, Eberhard Karls University of Tübingen, Tübingen, Germany

¹⁰Thermo Fisher Scientific, Bordeaux, France

¹¹Mammal Section, Department of Life Sciences, The Natural History Museum, London, UK

¹²Institut Universitaire de France (IUF), Paris, France

¹³Division of Vertebrate Zoology (Mammalogy), American Museum of Natural History, New York, New York, USA

Correspondence

Quentin Martinez, Staatliches Museum für Naturkunde Stuttgart DE-70191, Stuttgart, Germany.
Email: quentinmartinezphoto@gmail.com

Funding information

SYNTHESYS+, Grant/Award Number: GB-TAF-1316; Agence Nationale de la Recherche, Grant/Award Numbers: DS10, ANR-17-CE02; Alexander von Humboldt-Stiftung, Grant/Award Number: 1222365; Bundesministerium für Bildung und Forschung, Grant/Award Number: 05D2022; European Research Council consolidator grant, Grant/Award Number: ConvergeAnt; ERC-2015-CoG-683257, PI F. Delsuc; French National Research Agency, Grant/Award Number: CEBA: ANR-10-LABX-25-01

Abstract

Turbinals are key bony elements of the mammalian nasal cavity, involved in heat and moisture conservation as well as olfaction. While turbinals are well known in some groups, their diversity is poorly understood at the scale of placental mammals, which span 21 orders. Here, we investigated the turbinal bones and associated lamellae for one representative of each extant order of placental mammals. We segmented and isolated each independent turbinal and lamella and found an important diversity of variation in the number of turbinals, as well as their size, and shape. We found that the turbinal count varies widely, from zero in the La Plata dolphin, (*Pontoporia blainvillei*) to about 110 in the African bush elephant (*Loxodonta africana*). Multiple turbinal losses and additional gains took place along the phylogeny of placental mammals. Some changes are clearly attributed to ecological adaptation, while others are probably related to phylogenetic inertia. In addition, this work highlights the problem of turbinal nomenclature in some placental orders with numerous and highly complex turbinals, for which homologies are extremely difficult to resolve. Therefore, this work underscores the importance of

This is an open access article under the terms of the [Creative Commons Attribution-NonCommercial](https://creativecommons.org/licenses/by-nc/4.0/) License, which permits use, distribution and reproduction in any medium, provided the original work is properly cited and is not used for commercial purposes.

© 2024 The Author(s). *The Anatomical Record* published by Wiley Periodicals LLC on behalf of American Association for Anatomy.

developmental studies to better clarify turbinal homology and nomenclature and provides a standardized comparative framework for further research.

KEYWORDS

comparative anatomy, evolution, nasal cavity, olfaction, thermoregulation

1 | INTRODUCTION

The evolutionary success of mammals is often linked to their ability to maintain a stable internal body temperature, regardless of external environmental fluctuations. This adaptive trait allows mammals to inhabit a wide range of ecological niches that are often inaccessible to ectothermic organisms (Lovegrove, 2012). Furthermore, their highly developed sensory systems, particularly olfaction, are thought to have played a pivotal role in their survival, influencing crucial behaviors such as reproduction and foraging (Evans, 2003; Martinez et al., 2018; Stoddart, 1980; Yohe et al., 2022). These two key factors in the mammalian diversification, temperature regulation and olfaction, are enabled, to some extent by turbinals (= scrolled or branched bones within the nasal cavity).

In the anterior region of the nasal cavity, the respiratory turbinals are lined with a highly vascularized mucosa with ciliated epithelium and mucous glands involved in heat and moisture retention (Martinez, Amson, Ruf, et al., 2024; Negus, 1958). When air is inhaled, it comes into contact with the vascularized anterior portion of the respiratory turbinals, where it is warmed to body temperature. In the meantime, contact with nasal mucus moistens the air. During exhalation, this warmed air is cooled by the anterior part of the respiratory turbinals, which were previously cooled by the incoming air. This decrease in temperature causes water from the nasal cavity to condense, resulting in the expulsion of drier air (Collins et al., 1971; Jackson & Schmidt-Nielsen, 1964; Schmidt-Nielsen et al., 1970). In the posterior region of the nasal cavity, the olfactory turbinals are involved in olfaction (Martinez, Amson, Ruf, et al., 2024; Negus, 1958) and are lined with an olfactory epithelium containing olfactory receptor neurons (Martinez, Amson, Ruf, et al., 2024; Negus, 1958; Smith et al., 2004; Yee et al., 2016). When odor molecules enter the nasal cavity through inhalation or sniffing, part of these molecules are trapped in the olfactory epithelium, and the information is transmitted to and processed in the olfactory bulbs via cilia, olfactory receptors, and olfactory nerves. This sensory information is then further processed in other parts of the brain, such as the olfactory cortex (Wilson & Sullivan, 2011).

Respiratory and olfactory turbinals have been shown to be associated with ecological adaptation in mammals (Martinez et al., 2020; Van Valkenburgh et al., 2011). For instance, the development and complexity of turbinals have been linked to diet (Martinez et al., 2018; Melin et al., 2022) or aquatic adaptation (Green et al., 2012; Martinez et al., 2020; Martinez, Courcelle, et al., 2023; Martinez, Okrouhlik, et al., 2023; Van Valkenburgh et al., 2011, 2014). Turbinal anatomy has been best documented in bats (e.g., Bhatnagar & Kallen, 1974; Giannini et al., 2012; Ito et al., 2021; Smith et al., 2012, 2022; Smith, Corbin, et al., 2021; Smith, Craven, et al., 2021), primates (Lundeen & Kirk, 2019; Maier & Ruf, 2014; Smith et al., 2004; Smith & Rossie, 2008; Smith, Rossie, & Bhatnagar, 2007), some carnivores (Green et al., 2012; Van Valkenburgh et al., 2011, 2014; Wagner & Ruf, 2019, 2021), some rodents (Martinez et al., 2018, 2020; Martinez, Courcelle, et al., 2023; Ruf, 2020; Smith & Bonar, 2022), some eulipotyphlans (Ganeshina et al., 1957; Ito et al., 2022; Martinez et al., 2020; Woehrmann-Repenning & Meinel, 1977), and in marsupials (Macrini, 2012, 2014; Macrini et al., 2023; Rowe et al., 2005). Apart from seminal works on a limited number of species (Fawcett, 1921; Fischer, 1901; Paulli, 1900a; Paulli, 1900b; Paulli, 1900c; Starck, 1960; Voit, 1909), some orders have been clearly neglected, especially at the adult stage. There are several reasons for this, including the fact that access to turbinals was extremely cumbersome and destructive, prior to the advent of computed tomography (CT) technology. Large skulls are still challenging to scan, due to technical limitations associated with high-resolution CT-scanners. More importantly, some species have numerous and highly complex turbinals, making the segmentation process very tedious and time consuming. To fill this gap and better understand the evolution and diversity of the turbinal number and complexity in adult placental mammals, we isolated each turbinal individually in one species from each order of placental mammals. We then proposed an attempt to establish turbinal homologies across the sampled species. This study aimed to provide a standardized comparative anatomical framework that can serve as a potential basis for future research.

2 | MATERIALS AND METHODS

Twenty-one species, representing all extant orders of placental mammals, were studied (Figures 1 and 2). X-ray micro-computed tomography (μ CT) data were acquired for this study or were available on MorphoSource (see S11). Individuals were selected based on their turbinal preservation as well as the availability of specimens or CT data. This dataset was built selecting one species per

order of placental mammals, which may not be representative of the diversity of the entire order. For the anterior part of the respiratory turbinals, which can be difficult to assess for damage, we thoroughly examined other CT data and skulls whenever possible to ensure accuracy. Additional individuals from the species presented in this study, as well as other species, were examined to provide a broader overview and confirm some of the patterns discussed herein.

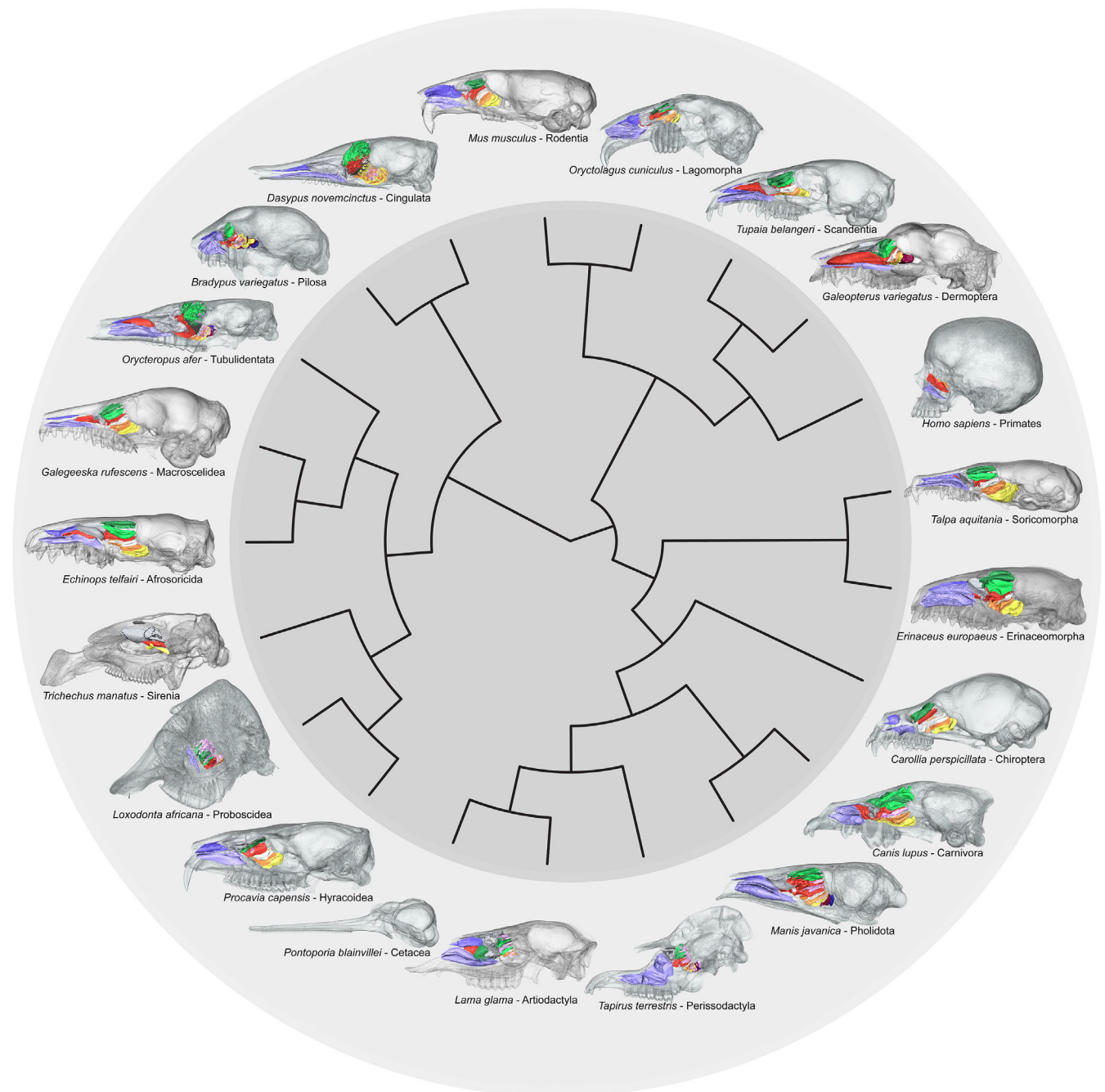


FIGURE 1 Sagittal views of the skull and segmented turbinals representing the diversity of turbinal bones across 21 orders of placental mammals. Colors correspond to potential turbinal homologies. Tree topology after Upham et al. (2019). Skulls and 3D renderings not to scale.

			nt	sl	mt	fts	ets
<i>Mus musculus</i> - Rodentia			1	1	1	1 (incl. 0it)	4 (incl. 1Tit and 0it)
<i>Oryctolagus cuniculus</i> - Lagomorpha			1	1	1	3 (incl. 1it)	3-4 (incl. 0-1Tit and 0it)
<i>Tupaia belangeri</i> - Scandentia			1	1	1	2 (incl. 0it)	4 (incl. 1Tit and 0it)
<i>Galeopterus variegatus</i> - Dermoptera			1?	1	1	2 (incl. 0it)	5 (incl. 1Tit and 0it)
<i>Homo sapiens</i> - Primates			0	0	1	0 (incl. 0it)	2 (incl. 0Tit and 0it)
<i>Talpa aquitania</i> - Soricomorpha			1	1	1	2 (incl. 0it)	4 (incl. 1Tit and 0it)
<i>Erinaceus europaeus</i> - Erinaceomorpha			1	1	1	2 (incl. 0it)	4 (incl. 1Tit and 0it)
<i>Carollia perspicillata</i> - Chiroptera			1	1	1	1 (incl. 0it)	4 (incl. 1Tit and 0it)
<i>Canis lupus</i> - Carnivora			1	1	1	8 (incl. 4its)	5 (incl. 1Tit and 1it)
<i>Manis javanica</i> - Pholidota			1	1	1	7 (incl. 3its)	9 (incl. 1Tit and 3its)
<i>Tapirus terrestris</i> - Perissodactyla			0?	1	1	18-21 (incl. 13-16its)	23-25 (incl. 1Tit and 17-19its)
<i>Lama glama</i> - Artiodactyla			1?	1	1	10 (incl. 6its)	8-10 (incl. 1Tit and 3-5its)
<i>Procavia capensis</i> - Hyracoidea			1	1	1	1-2 (incl. 0-1it)	4 (incl. 1Tit and 0it)
<i>Loxodonta africana</i> - Proboscidea			0?	1	1	34 (incl. 30its)	19 (incl. 1Tit and 15its)
<i>Trichechus manatus</i> - Sirenia			1?	1	0	0 (incl. 0it)	4 (incl. 1Tit and 0it)
<i>Echinops telfairi</i> - Afrosoricida			1	1	1	2 (incl. 0it)	4 (incl. 1Tit and 0it)
<i>Galegeeska rufescens</i> - Macroscelidea			1	1	1	2 (incl. 0it)	4 (incl. 1Tit and 0it)
<i>Orycteropus afer</i> - Tubulidentata			1	1	1	32 (incl. 21its)	14 (incl. 1Tit and 8its)
<i>Bradypus variegatus</i> - Pilosa			1	1	1	4 (incl. 2its)	12 (incl. 1Tit and 6its)
<i>Dasybus novemcinctus</i> - Cingulata			1	1	1	16 (incl. 10its)	22 (incl. 1Tit and 12its)

FIGURE 2 Details of the turbinals in lateral (left) and medial (right) views, along with their count (for only one side), across placental mammal orders. 3D renderings not to scale.

In most species (see SI1), bony elements from one side of the skull were isolated using the structure enhancement filter option in Avizo 3D 2021.2 (Thermo Fisher Scientific). Threshold values were adjusted in each species to better match the actual turbinal bony thickness. The turbinals were then manually isolated from the other bony elements, and the segmentation was refined. In some species, turbinals were manually segmented (see SI1).

In this study, we used the terminology of fronto- and ethmoturbinals adapted from Paulli (1900a), Paulli (1900b), and Paulli (1900c) (see also Maier, 1993; Voit, 1909) and based on homology determined by developmental studies (e.g., Ito et al., 2021, 2022; Macrini, 2014; Macrini et al., 2023; Ruf, 2020; Smith et al., 2023; and see review in Martinez, Amson, Ruf, et al., 2024). The colored turbinal renderings and legends as displayed in the figures represent the hypothesized identification and delimitation (Figures 1–14). However, alternative hypotheses may be discussed or proposed. For example, dark gray colors annotated as “unidentified lamella” convey uncertainty (discussed in the text), and dashed lines on the semicircular lamella of *Trichechus manatus* (Figure 10) and on the nasoturbinal of *Lama glama* (Figure 9) represent potential sutures indicative of alternative delimitations. In most species, turbinal colors represent likely turbinal homology across species; however, in species with numerous turbinals that are intricately intertwined, the homology remains unclear (see discussion) and colors mostly represent the order of appearance from the most medio-dorsal to the most medio-ventral turbinal. This is for example the case for *Dasypus*, *Loxodonta*, and *Orycteropus*.

The nasoturbinal (nt), the semicircular lamina (sl), and the maxilloturbinal (mt) have a uniquely defined color across species according to potential turbinal homology (nt is dark purple, sl is gray, and mt is light purple). From the most medio-dorsal to the most medio-ventral order, the frontoturbinals (*fts*) were alternatively colored with two nuances of green. Here, we assigned the turbinal directly dorsal to the ethmoturbinal I (*etI*) as a frontoturbinal or an interturbinal (*it*) from the group of frontoturbinals. Thus, in this study, the *etI* represents the first ethmoturbinal. Here, the pars anterior (*pa*) and pars posterior (*pp*) of the ethmoturbinal I (*etI*) were colored in red. The reader should be aware that what is referred to here as *etI pa* and *etI pp* are also named *etI* and *etII* by some other authors (see review in Martinez, Amson, Ruf, et al., 2024). From the *etI pp* up to the medioventral-most turbinal, all turbinals were considered to represent ethmoturbinals. They were independently colored from *etI* to *etVI* with potential homology. In *Dasypus novemcinctus*, where numerous ethmoturbinals are present, the

ethmoturbinals were colored sequentially with alternating orange and yellow colors (Figure 13).

In an attempt to follow the common definition of interturbinals (see Martinez, Amson, Ruf, et al., 2024), we considered interturbinals to be less developed fronto- or ethmoturbinals that did not extend as far (especially medially) as others. In species with numerous fronto- and ethmoturbinals, as well as complex turbinals, such definition is difficult to apply objectively (see Discussion), and many were defined using 3D rendering. For *Canis* (Figure 7), the attribution does not only follow this common definition, as it was based on Wagner and Ruf (2019), who documented multiple developmental stages (but see Figure 7 and result section about the identified frontoturbinal 4). All the attributions were performed by a single operator. All but one of the interturbinals were similarly colored. Among the interturbinals, one has received more attention than the others in several studies (e.g., Smith, Bhatnagar, et al., 2007; Smith, Rossie, & Bhatnagar, 2007; Smith, Corbin, et al., 2021; Smith, Craven, et al., 2021 and see Martinez, Amson, Ruf, et al., 2024), and there is potential homology for this interturbinal across species (see Martinez, Amson, Ruf, et al., 2024). This interturbinal, generally located between *etI* and *etII*, is referred to here as the *main it* and is colored white. When this homology was unclear, the *main it* was identified as the first relatively large interturbinal directly ventral to the *etI pp*. In this study, in the coronal plane, all turbinals located ventrally to ethmoturbinal I (*etI*) are considered ethmoturbinals. This definition, therefore, includes the interturbinals from this morphological space (including the “main” interturbinal). However, in the figures, these turbinals are named based on their potential homology, distinguishing between the ethmoturbinals and interturbinals (see review in Martinez, Amson, Ruf, et al., 2024. for a thorough discussion about turbinal identification and counting).

In this study, we employed the term “recess” to encompass all the cavities shaped by the turbinals, which may be open or closed. However, it is likely that some of these recesses could be classified as sinuses (see Billet et al., 2017). The following description covers only one side of the skull (inconsistently left or right side) and therefore only half of all the turbinals. In addition, the cetacean *Pontoporia blainvillei* displayed no identifiable turbinal and is not described below. Except if explicitly stated, turbinals are described in the result section in the coronal plane from anterior to posterior.

For the figured timetree, we used the phylogeny of maximum clade credibility (MCC) obtained from 10,000 trees sampled in the posterior distribution of Upham et al. (2019) and pruned it to match the species sampled in our dataset (Figures 1 and 2). For illustrative purposes, the species *Talpa europaea* was replaced by *Talpa aquitania*, as the

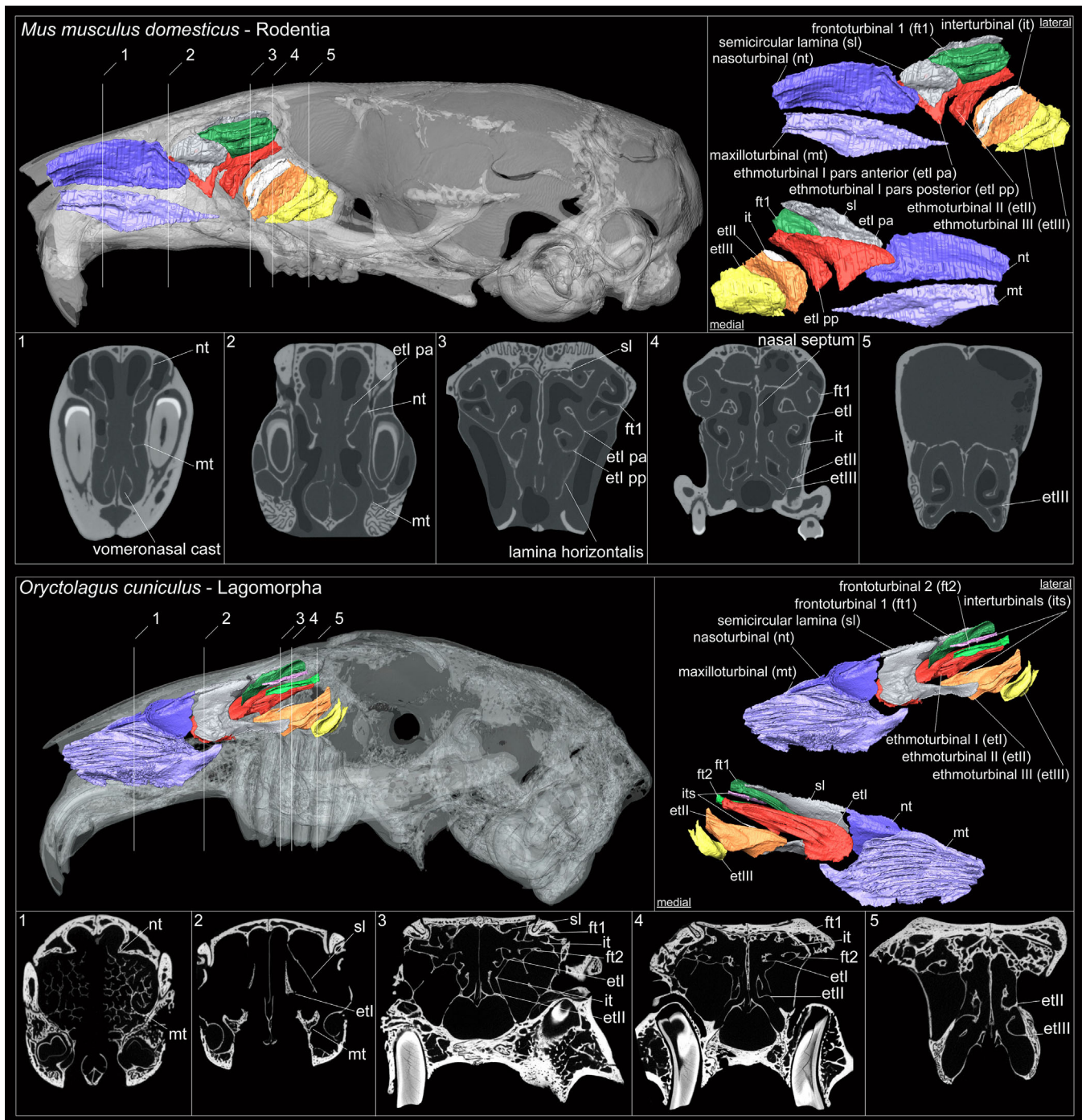


FIGURE 3 Sagittal views of the skull and segmented turbinals, along with coronal sections of the nasal cavity, illustrating a mouse (*Mus musculus domesticus*, wild individual from Monastir, Tunisia, ISEM K7503) and a European rabbit (*Oryctolagus cuniculus*, DU BAA 0021). Skulls and 3D renderings not to scale.

latter is missing from the phylogeny used. The MCC consensus tree was inferred using TreeAnnotator v.1.8.284 (Bouckaert et al., 2014) with a 25% burn-in. When performing the 3D rendering, some thin turbinals artificially showed large holes due to smoothing parameters. To be consistent with the actual segmentation and anatomical reality, such large holes were sometimes artificially filled in Photoshop for illustrative purposes only.

3 | RESULTS

3.1 | General comparative description

3.1.1 | Nasoturbinal and semicircular lamina

The relative size of the nasoturbinal (*nt*) shows some variation among species, but is generally present as an

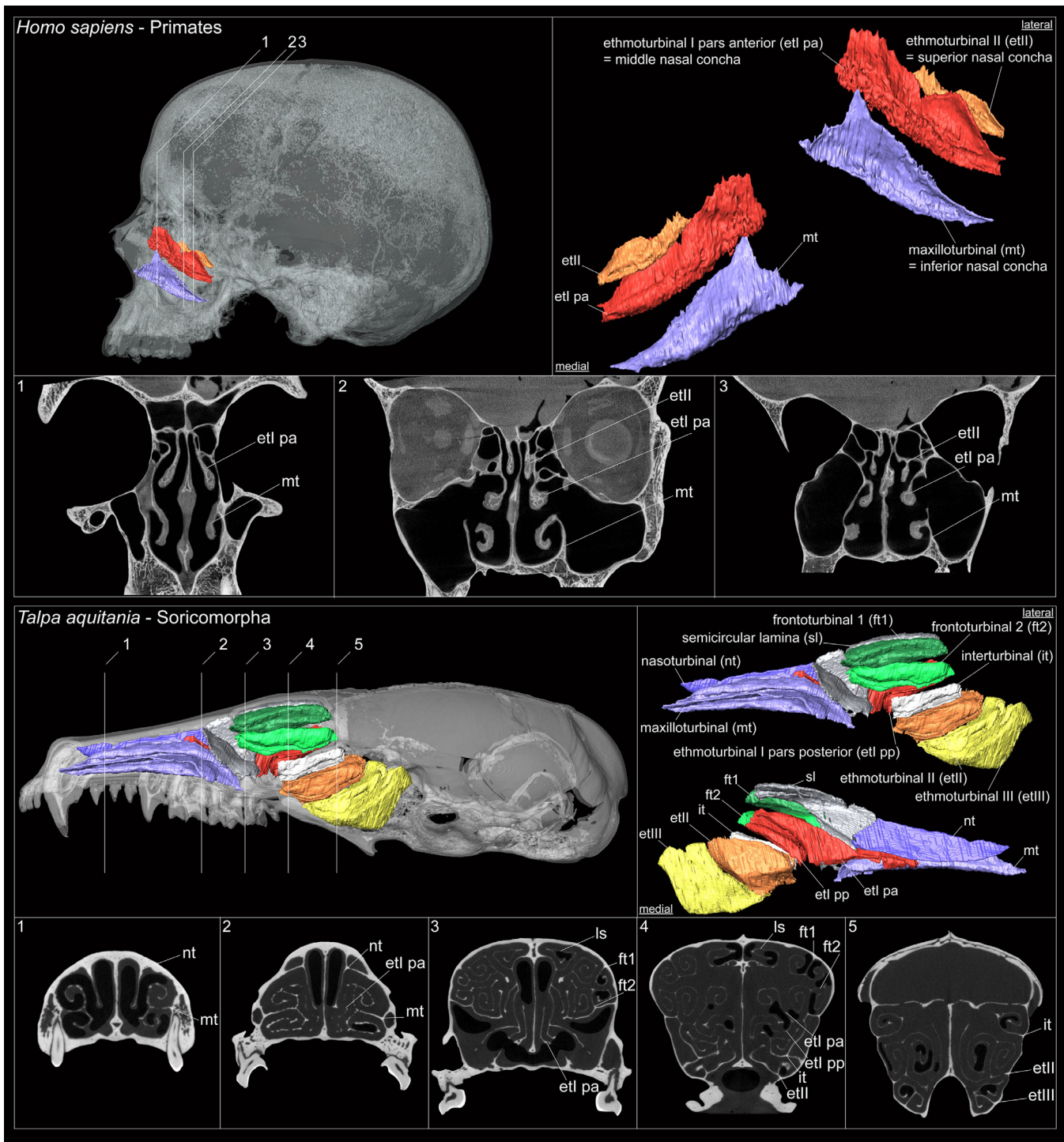


FIGURE 5 Sagittal views of the skull and segmented turbinals, along with coronal sections of the nasal cavity, illustrating a human (*Homo sapiens sapiens*) and an Aquitanian mole (*Talpa aquitania*, ISEM QM). Skulls and 3D renderings not to scale.

3.1.2 | Maxilloturbin

As previously described (Martinez, Okrouhlik, et al., 2023), the maxilloturbin (*mt*) shows significant variation among mammals. In our sample, the *mt* might only be lost in *Trichechus* and *Pontoporia* (Figures 1, 10).

Some species display highly complex *mt*, such as *Oryctolagus*, *Erinaceus*, and *Canis* (Figures 3, 6, and 7). Others have highly developed but noncomplex *mt*, such as *Manis*, *Tapirus*, *Lama*, *Orycteropus*, and *Bradypus* (Figures 8, 9, and 12). In *Loxodonta*, the *mt* presents a unique dorso-ventral orientation (Figure 10).

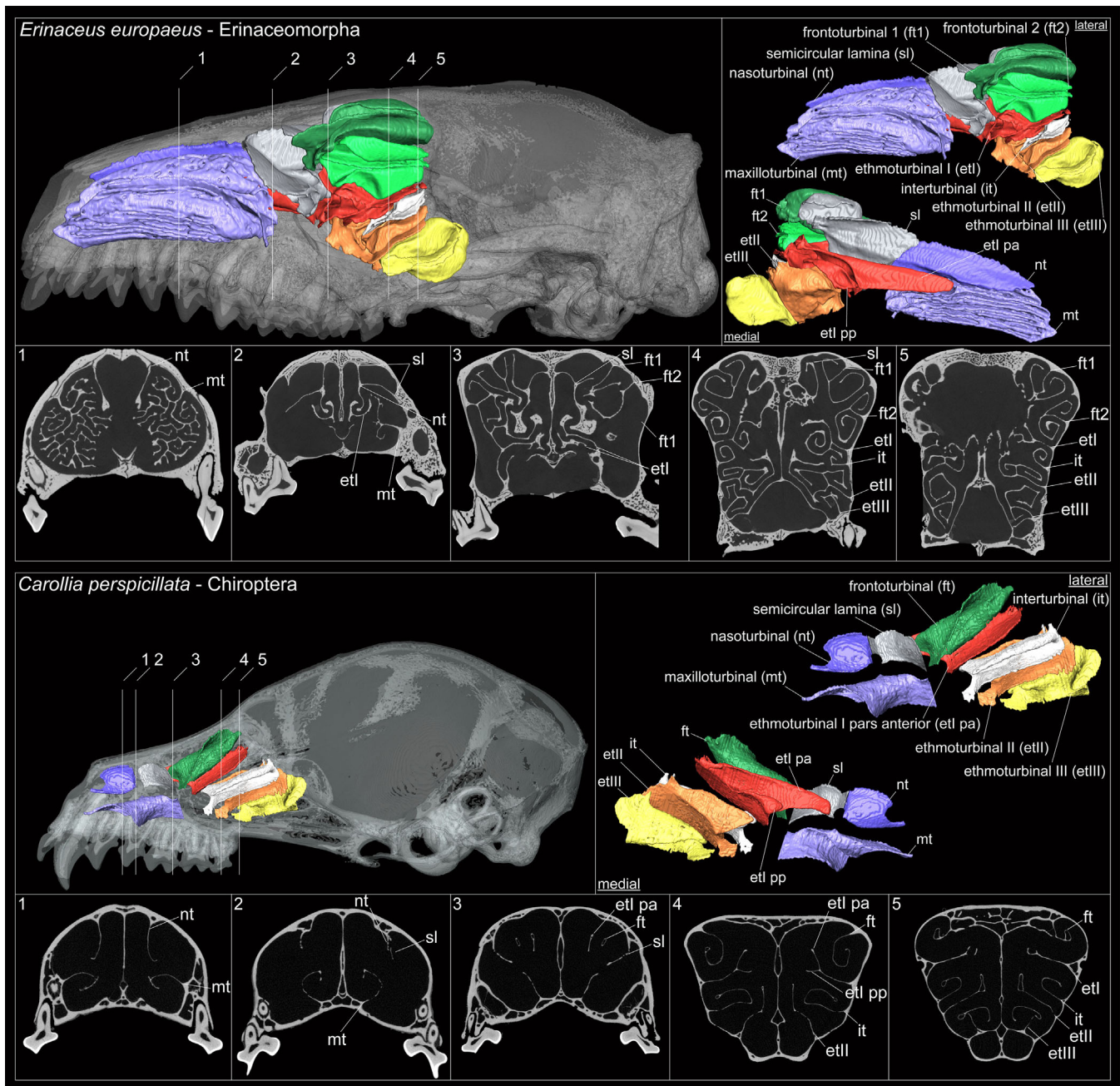


FIGURE 6 Sagittal views of the skull and segmented turbinals, along with coronal sections of the nasal cavity, illustrating an European hedgehog (*Erinaceus europaeus*, NHMUK 1958 60 212) and a Seba's short-tailed bat (*Carollia perspicillata*, NHMUK 66 3432). Skulls and 3D renderings not to scale.

3.1.3 | Frontoturbinals and interturbinals

The number of frontoturbinals (*fts*), including the interturbinals (*its*), varies from 0 in *Homo* and *Pontoporia* (and possibly in *Trichechus*, Figures 5 and 10) to 34 in *Loxodonta* (Figure 10). In *Galeopterus*, but more impressively in *Lama*, the *fts* and *its* form large recesses (Figures 4 and 9). Also, in *Lama*, the potential anterior part of the *ft3* extends extremely far anteriorly. In *Orycteropus* and *Dasybus*, the *fts* and *its* are intricately intertwined (Figures 12, 13, and 14). In taxa with a very large number of *its*, such as *Loxodonta*,

Orycteropus, and *Dasybus*, it is difficult to ascertain the turbinal number due to fusion with several lamellae at different points (Figures 10, 12, 13, and 14). In species with numerous or complex *fts* and *its*, attribution to *ft* or *it* is difficult and mostly based on 3D rendering.

3.1.4 | The ethmoturbinal I

The ethmoturbinal I (*etI*) shows some variation across species in terms of its extension into the nasal cavity. In

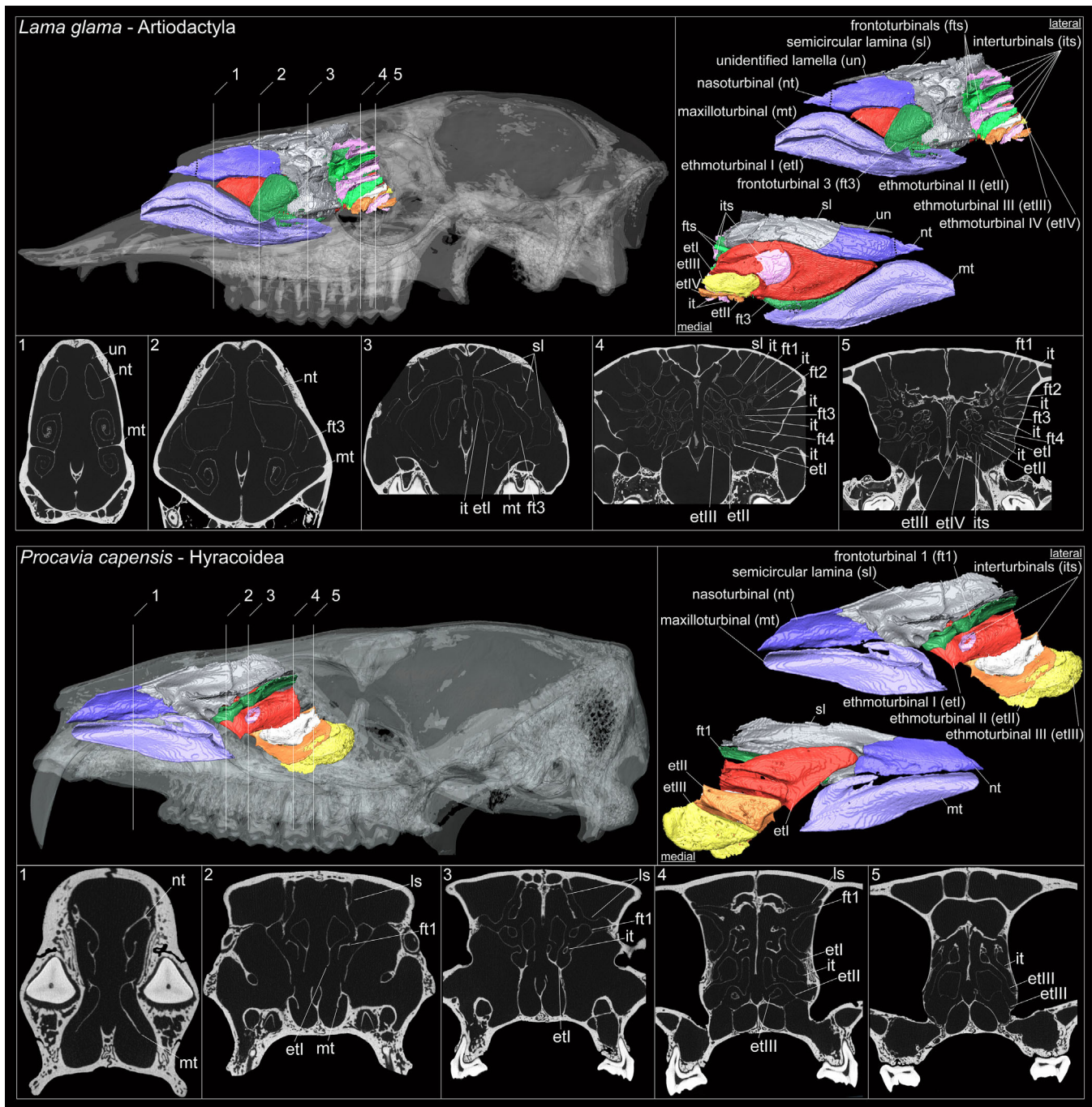


FIGURE 9 Sagittal views of the skull and segmented turbinals, along with coronal sections of the nasal cavity, illustrating a llama (*Lama glama*, USNM 278681) and a rock hyrax (*Procavia capensis*, umzc H5081A). Skulls and 3D renderings not to scale.

3.1.5 | Ethmoturbinals and interturbinals

The number of ethmoturbinals (*ets*), including the interturbinals (*its*), varies from two in *Homo* (excluding *Pontoporia* where none are present) to 23–25 in *Tapirus* (Figures 5, 8, and 14). Species with a large number of turbinals also tend to be more complex in shape, forming numerous scrolls and resulting in

densely packed turbinals with minimal space between them. This is the case, for example, in *Loxodonta*, *Orycteropus*, and *Dasyus* (Figures 10, 12, 13, and 14). In these species, objective attribution to *its* or *ets* remains difficult, but less so than in frontoturbinals. Interestingly, there are some variations in the proportions of *ets* and *its*. For example, *Dasyus* has 9 *ets* and 13 *its* (including the “main” interturbinal (*main*

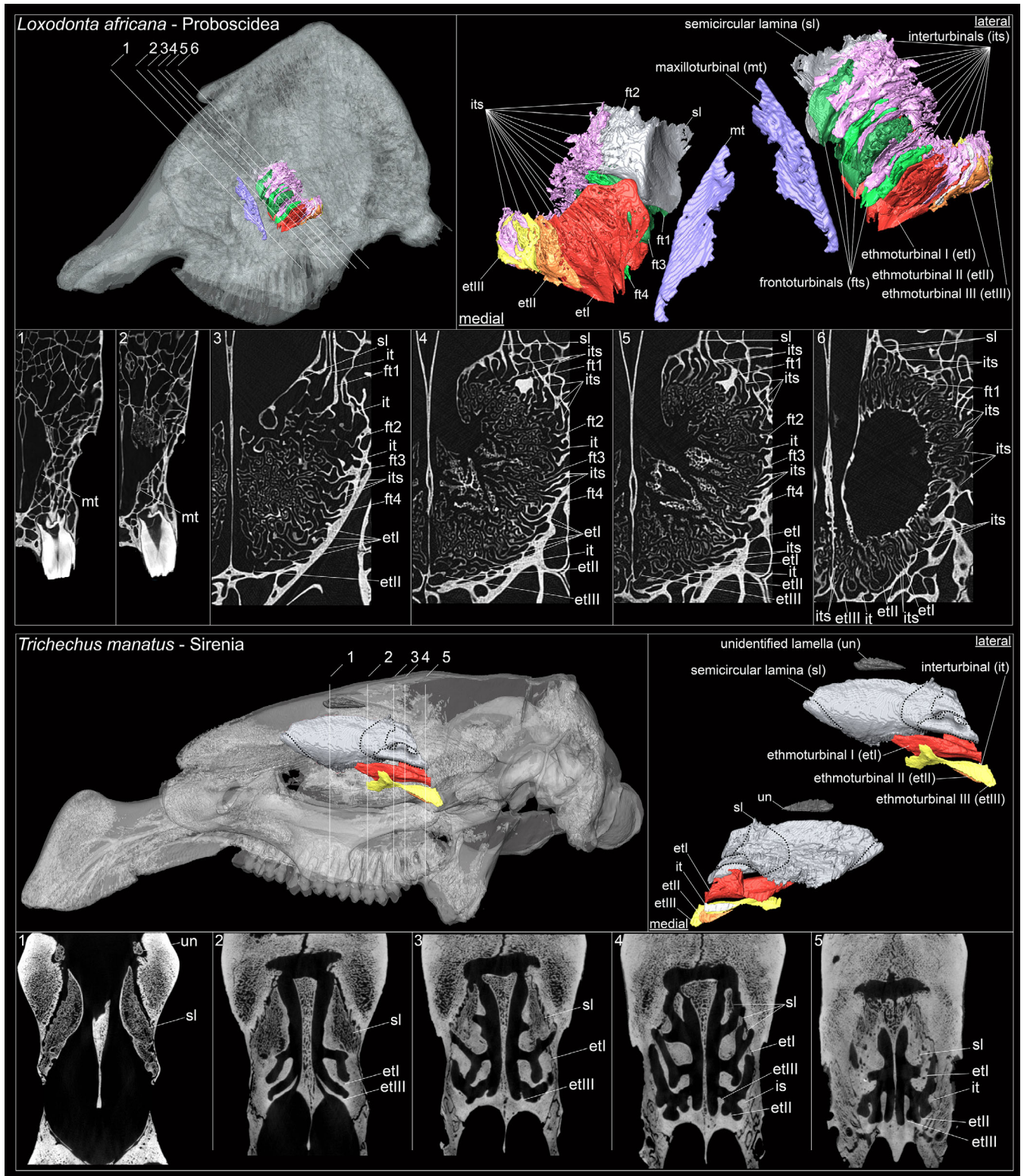


FIGURE 10 Sagittal views of the skull and segmented turbinals, along with coronal sections of the nasal cavity, illustrating an African bush elephant (*Loxodonta africana*, LACM 52471) and a West Indian manatee (*Trichechus manatus*, SMNS-Z-MAM-1125). Skulls and 3D renderings not to scale.

it), Figures 13 and 14), and *Loxodonta* has 16 its (including the main it, Figures 10 and 14) but only 3 ets. However, the exact delimitation of the its is more difficult in *Loxodonta* than in *Dasyus*,

potentially explaining some of these differences. As with the other olfactory turbinals, the ethmoturbinals of *Galeopterus* and *Lama* show a unique pattern of recesses (Figures 4, 9).

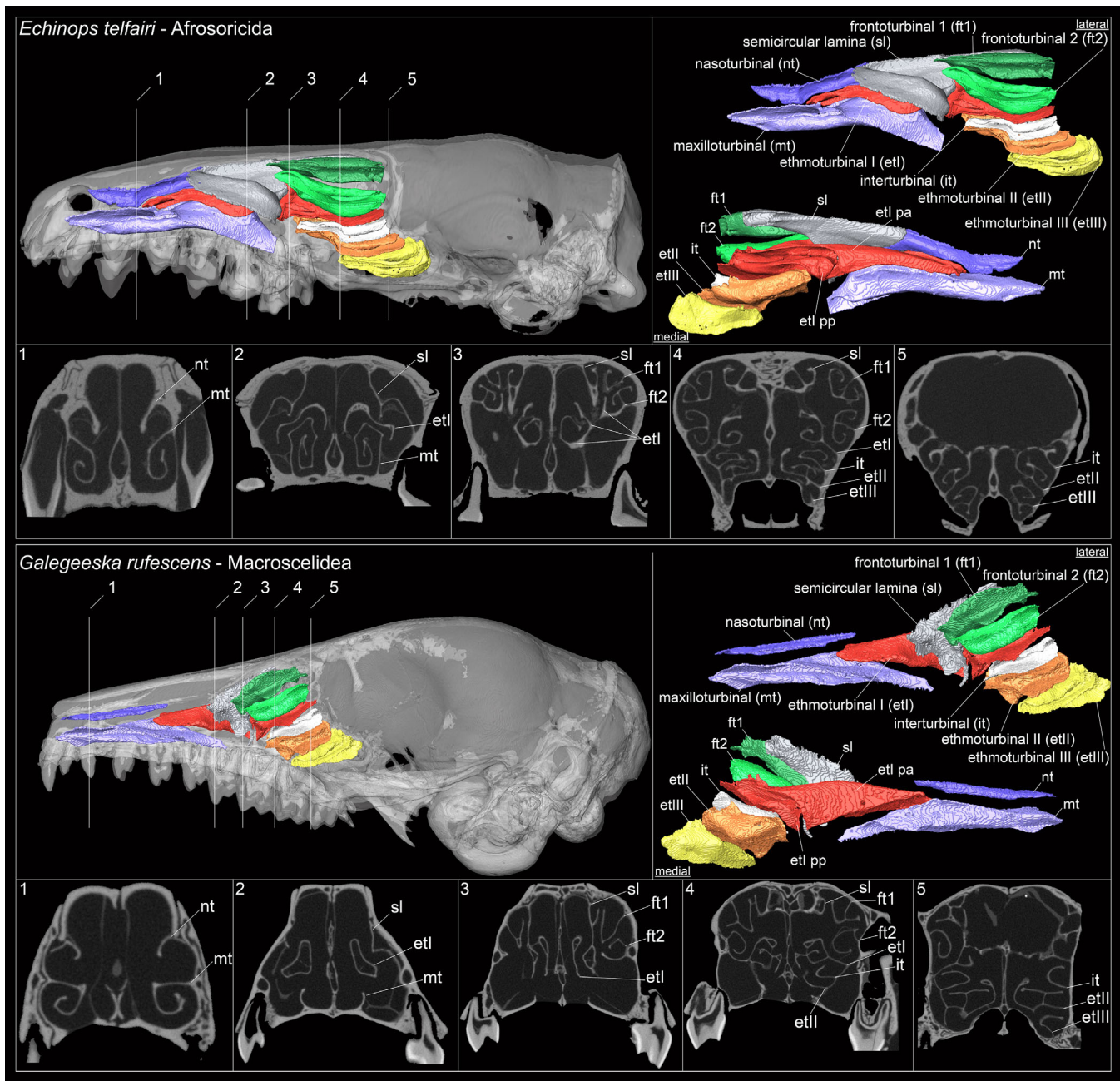


FIGURE 11 Sagittal views of the skull and segmented turbinals, along with coronal sections of the nasal cavity, illustrating a lesser hedgehog tenrec (*Echinops telfairi*, NHMUK 921164) and a rufous elephant shrew (*Galegeeska rufescens*, AMNH 118885). Skulls and 3D renderings not to scale.

3.1.6 | The “main” interturbinal

The “main” interturbinal (*main it*) is only absent in *Pontoporia* and *Homo* (Figure 5) and in some individuals of *Oryctolagus*, either on one side or both (=intra individual variation, Figure 3). In species with a low number of ethmoturbinals, the identification of the *main it* is generally straightforward. However, in species where the exact posterior delimitation of the *etI* is unclear, such as *Orycteropus* or *Dasyopus*, the identification of the *main it* remains unclear (Figures 12, 13, and 14). In *Loxodonta*, other smaller interturbinals lie between the larger interturbinal

identified as the *main it*, but its homology remains hypothetical (Figures 10 and 14). In *Galeopterus*, *Lama*, and *Procavia*, the *main it* forms a recess (Figures 4 and 9).

3.2 | Detailed anatomical descriptions

3.2.1 | Nasoturbinal and semicircular lamina

Mus—The nasoturbinal (*nt*) emerges dorsally and rapidly forms a laterally oriented scroll with an additional small ventrally oriented lamella. The *nt* migrated

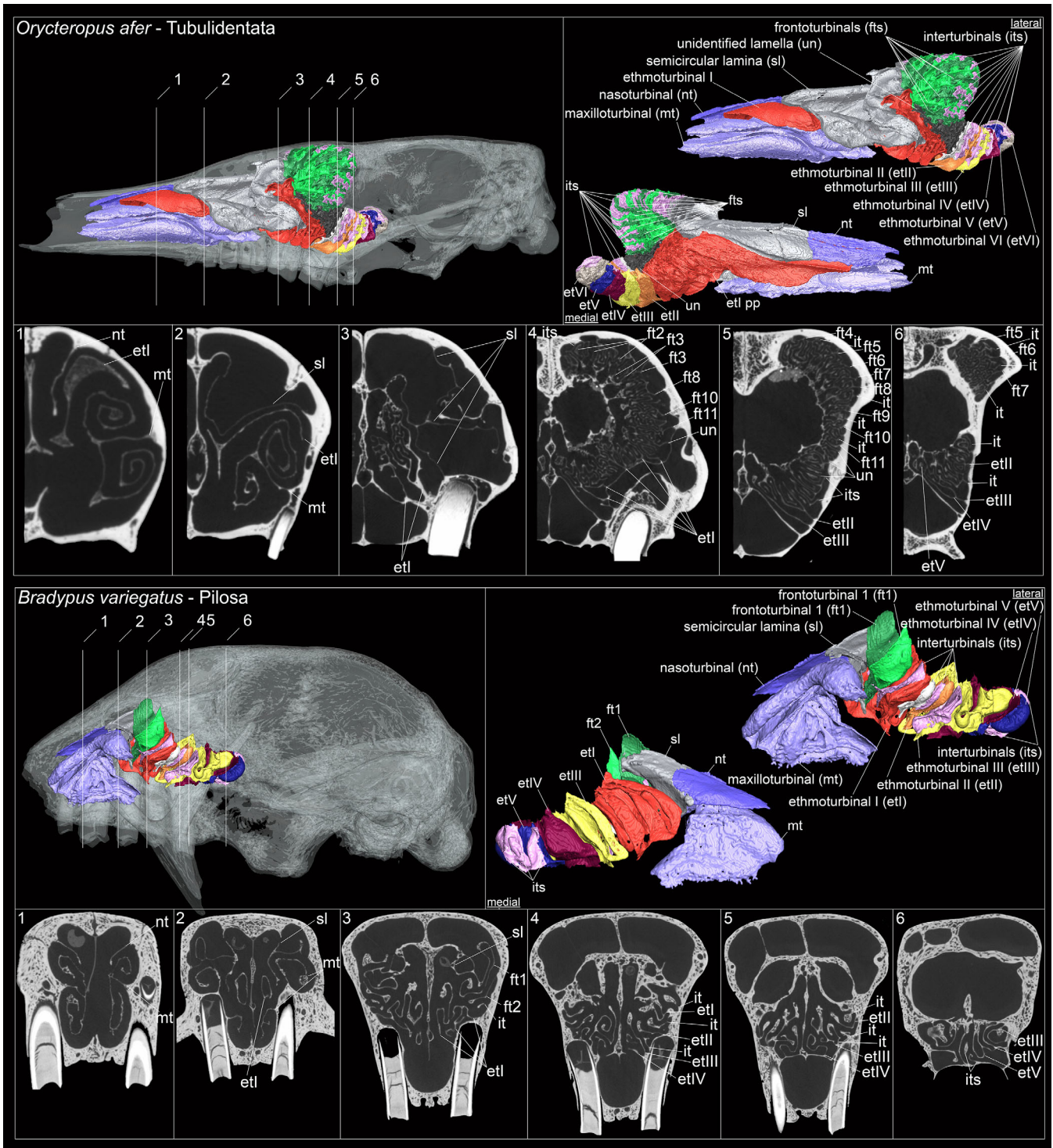


FIGURE 12 Sagittal views of the skull and segmented turbinals, along with coronal sections of the nasal cavity, illustrating an armadillo (*Orycteropus afer*, NHMUK 29958) and brown-throated sloth (*Bradypus variegatus*, USNM 549523). Skulls and 3D renderings not to scale.

laterally, reduced, and formed a small recess at its lateral root. The delimitation along its entire length is not difficult. The *nt* is in contact with the semicircular lamina (*sl*) but does not fuse with it, and a clear delimitation is visible. Posteriorly, the *sl* forms a recess between the lateral wall of the nasal cavity and the skull roof, then opens

and separates into the uncinata process (*up*) and the dorsal parts of the *sl*. The dorsal part forms a small recess at its ventralmost part and posteriorly forms a laterally scrolled lamella that fuses and ends with the cribriform plate. The *up* and the rest of the *sl* are separated by a small suture along their length and are clearly separated

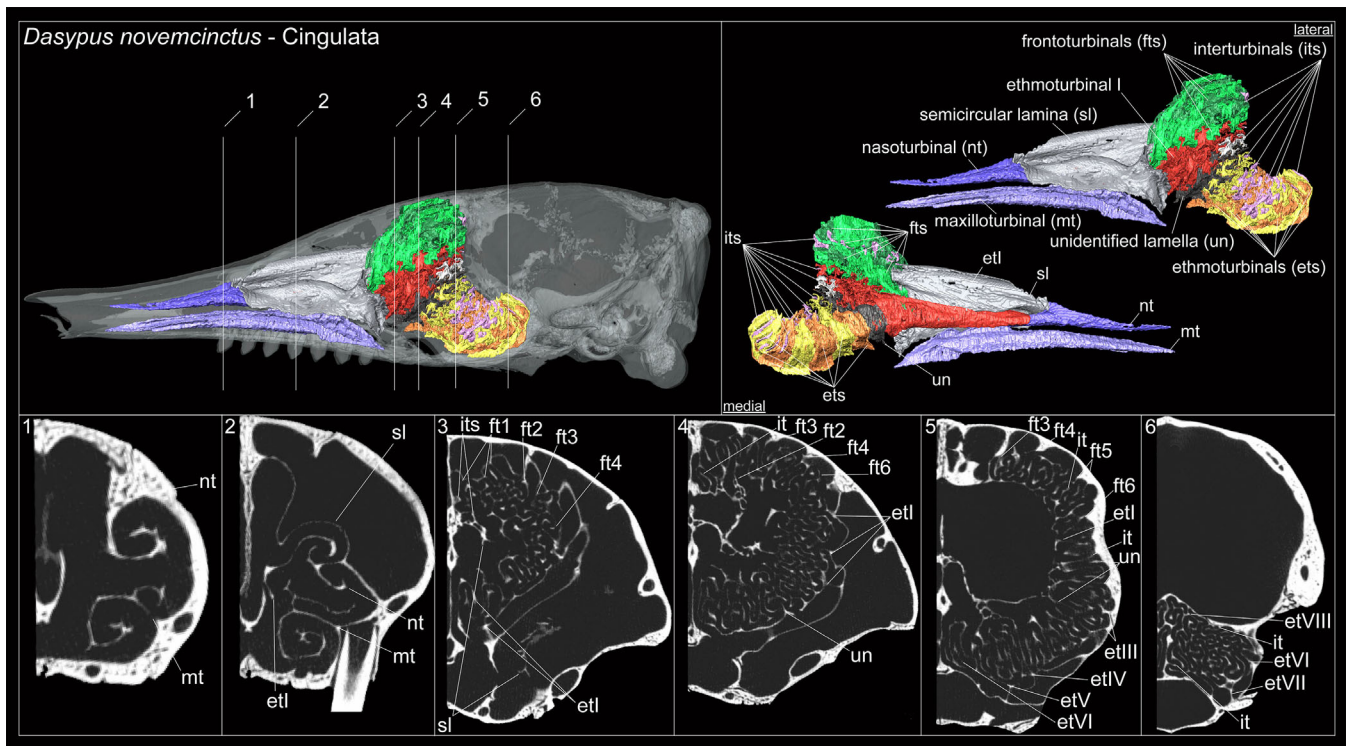


FIGURE 13 Sagittal views of the skull and segmented turbinals, along with coronal sections of the nasal cavity, illustrating a nine-banded armadillo (*Dasypus novemcinctus*, AMNH 263287). Skull and 3D renderings not to scale.

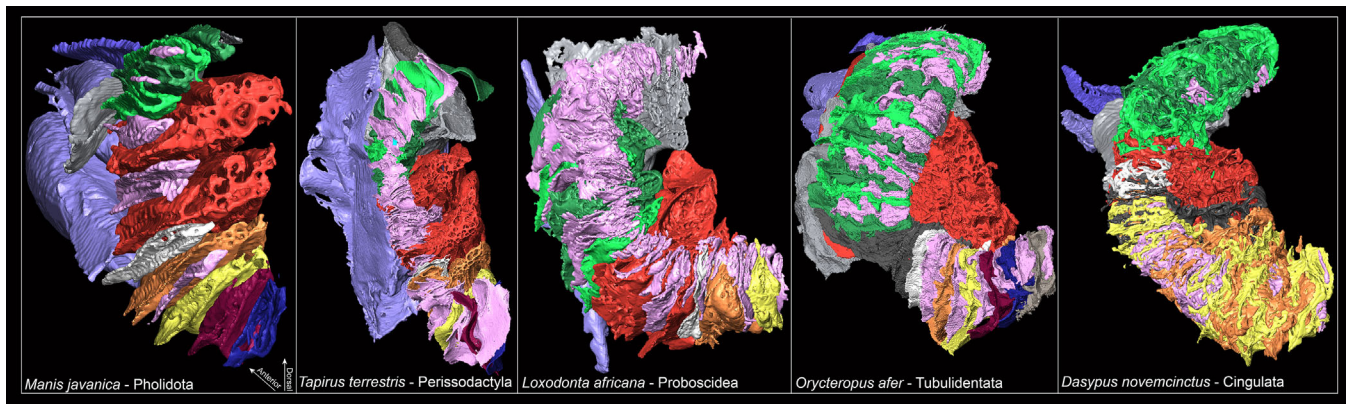


FIGURE 14 Posterior view of left turbinals in four mammalian species featuring a large number and/or a high complexity of turbinals, illustrating the intricate connections between some turbinals. 3D renderings not to scale.

from each other. The *up* attaches and ends at the posterior part of the incisor alveolus. ***Oryctolagus***—The *nt* starts relatively posteriorly with a very small lamella that is fused to the mid-ventral wall of the nasal, from which it is barely separated. Posteriorly, it extends to form a large recess from the skull roof to the lateral wall of the nasal cavity, then separates from it to end medially. The *sl* starts to develop where the *nt* almost completely ends; they display a continuity with almost no direct contacts (a very small gap). The delimitation between the *nt* and the *sl* is clear in both coronal and sagittal views. This

clear delimitation enables us to interpret the anterior and posterior parts as the *nt* and the *sl*, respectively (as seen in Ruf, 2014). However, in the absence of such a delimitation, we would have interpreted the anterior part forming the recess (here identified as *nt*) as the *sl*, because it shows a similar morphological pattern as in other genera (e.g., *Mus*, *Galeopterus*, *Tupaia*, *Talpa*, *Erinaceus*, *Manis*). The *sl* is composed of a long, ventrally oriented lamina that is extremely thick in its ventralmost part. Then it divides into two parts, where the *up* is composed of a small lamella with a circular shape at its medial end,

which forms a small recess. The dorsal part of the *sl* attaches laterally and forms a recess that closes and then forms a scrolled lamella that ends medial to the skull roof. ***Tupaia***—The *nt* is composed of a small and simple lamella that slightly scrolls laterally, and that forms a small closed recess at its most lateral part. It then divides into two parts. One forms the main lamella, which shifts ventro-laterally and ends at the base of the maxilloturbinal (*mt*). The other part, composed of a small recess, continues slightly posteriorly to open and fuse with the lateral wall of the nasal cavity. More posteriorly, the recess opens again and fuses close to the most ventro-lateral part of the *sl*. As seen in sagittal view, the second part of this recess might not represent an actual part of the *nt* but rather a different lamella. There is no contact between the *nt* and the *sl*. Posteriorly, the *sl* forms a recess between the lateral wall of the nasal cavity and the skull roof, then separates into the *up* and the dorsal parts of the *sl*. The dorsal part forms a laterally scrolled lamella and ends medially to the cribriform plate. This recess also forms the beginning of the horizontal lamina (*hl*). ***Galeopterus***—The potential *nt* consists of an extremely thin and small lamella that is only visible in a few slices in high resolution scans. This lamella defines a small recess on the lateral wall of the nasal cavity. As in *Tupaia*, there is a discontinuity between the anterior and posterior parts of the recess. In sagittal view, the attribution to the posterior part as *nt* or another lamella is less clear than in *Tupaia*. This is rendered even more difficult because this small recess formed by this lamella lies on the *sl* and is fused to it posteriorly. Posteriorly, the *sl* forms a recess between the lateral wall of the nasal cavity and the skull roof, then opens and divides into smaller recesses, one laterally likely formed by the *up* and one dorsally that ends close to the cribriform plate. In this species, the *sl* never displays the shape of a classical scrolled lamella. ***Homo***—No *nt* or *sl* were identified. ***Talpa***—The *nt* is a long, straight lamella that extends to a very ventral part of the nasal cavity. There is no clear delimitation or suture with the *sl*. However, the *nt* size decreases as the *sl* increases, both dorsally and ventrally. Although subtle, the contact between these bones is also visible in sagittal view. There is then a clear continuity between the *nt* and *sl*. The *sl* starts by forming a recess between the lateral wall of the nasal cavity and the skull roof, then opens and separates into the *up* and the dorsal parts of the *sl*. When both parts are separated, the bony surface of the *up* is very thick. The dorsal part of the *sl* forms the common lateral scroll, which ends with the cribriform plate. In addition, there is a second, slightly medio-ventrally scrolled lamella that originates from the laterally scrolled lamella. The segmentation of the *sl* is different from that of Martinez, Amson, Ruf, et al. (2024)

in order to be consistent with all the species segmented here and to take into account all the lamellae that are fused with the *sl*. ***Erinaceus***—The nasoturbinal of *Erinaceus* is extremely similar to that of *Talpa* except that the ventral part of its *nt* is particularly thick. The delimitation between the *nt* and *sl* is here proposed to be similar to that in *Talpa*. The *sl* is also very similar to that of *Talpa*. As the ventral part of the *sl* decreases in length, it becomes extremely thick. There is a clear continuity between the *nt* and the *sl*. ***Carollia***—The *nt* corresponds to a small lamella, slightly scrolled laterally. The continuity between the *nt* and the *sl* is clear in the coronal view. The *sl* originates from a small lateral lamella, which extends posterior to the *nt*. The small lamella then migrates laterally and fuses ventrally with the dorsal continuity of the maxilloturbinal (*mt*). It is difficult to determine whether the fused part includes the *up*. The *sl* is therefore very simple (absence of the lateral scroll that fuses with the cribriform plate). ***Canis***—The *nt* is a simple, almost straight, ventrally oriented lamella showing a slightly thicker ventral part. The delimitation with the skull roof is extremely clear. In some regions, the *nt* and the ethmoturbinal I (*etI*) are very close and may even be in contact. The delimitation between the *nt* and the *sl* is interpreted to be located where the lamella splits into two lamellae to form a recess (see also Wagner & Ruf, 2019). This delimitation is clearer in the sagittal view. Therefore, there is a clear continuity between the *nt* and the *sl*. The *sl* forms a recess in the medial part of the skull roof and the lateral wall of the nasal cavity, then rapidly develops into multiple large and complex lamellae. During this development, the main root of the *sl* migrates laterally in contact with the nasal septum. Posteriorly, the *sl* reduces to a laterally oriented scrolled lamella that ends close to the cribriform plate. ***Manis***—The *nt* is a very short but thick lamella, oriented first laterally and then ventrally, with a thicker bony structure in its ventralmost part. A clear suture is visible between the *nt* and the *sl* and corresponds to the area where the single lamella splits into two lamellae and forms a recess, confirming the observations made for *Canis*. There is then a clear continuity between the *nt* and *sl*. The *sl* forms a recess between the skull roof and the lateral wall of the nasal cavity. This recess opens posteriorly and divides into two parts, the *up* and the dorsal part that reduces in the classical laterally scrolled lamella. ***Tapirus***—We could not identify a *nt* with certainty. There is a small and thick lamella dorsal to the *sl*. However, the absence of a clear end or suture posteriorly and its continuity with the nasal septum suggest that it unlikely corresponds to the *nt*. Also, an absence of clear suture in the identified *sl* makes it difficult to separate it into two parts.

Inspection of the 3D rendering of the *sl* did not help defining a potential delimitation. An alternative hypothesis could be that the dorsal part of what we identified as the maxilloturbinal (*mt*) could turn out to be the *nt*. However, this part never separates from the ventral part or from the main root of the *mt*. Overall, given the current evidence, our hypothesis is that adult *Tapirus* lacks a *nt*. The *sl* forms a recess with the lateral wall of the nasal cavity, then forms a second recess located more medially. Both recesses merge to form a larger recess that opens and separates between the ventro-lateral *up* and the medio-dorsal part of the *sl*. The *up* migrates dorso-laterally and fuses with other lamellae that will form the potential frontoturbinals. The medial part forms a new recess with a laterally oriented scroll. This recess closes while forming a new long medially oriented lamella, where several small lamellae are attached. All these lamellae end and fuse with the cribriform plate. We considered all these additional lamellae as part of the *sl*, but they could also represent independent lamellae. **Lama**—Three different delimitations seem to exist between the potential *nt* and the *sl*, but none of them allows us to give a more probable interpretation. Anteriorly, the potential *nt* starts as a very small lamella, not yet attached to any roots, and shortly splits into two lamellae to form a recess (as seen, for example, in *Canis*). The location where the single lamella splits into two may correspond to the first delimitation. This recess attaches dorsally to a very small lamella and then opens into a larger recess where one attachment is dorsal and the other migrates laterally. Where the first recess opens into a larger recess could correspond to the second delimitation. This is visually consistent with the 3D rendering of *Canis*. However, the exact delimitation where it forms the second large recess remains arbitrary. Finally, a small unidentified lamella, which is the most dorsal lamella, may also be considered as the potential delimitation. We have suggested several interpretations, but in this case, having access to multiple high resolution scans as well as younger individuals may help to clarify this delimitation. Where the second recess opens, it attaches to multiple lamellae dorsally and laterally and forms several large recesses, which corresponds to a unique feature among the studied species. The *sl* then divides (as in most other species) into a ventral part and a medio-dorsal part, both forming a large recess. The large medio-dorsal recess ends in fusing with the cribriform plate. Due to its unique shape (not only related to the *sl*, see below), it is difficult to assign the various recesses and lamellae that are connected to it. **Procapra**—The *nt* is a laterally scrolled lamella with another additional ventrally oriented

lamella at its ventralmost part. The size of the *nt* appears to decrease when the *sl* increases in size and forms a recess with a dorsal and a lateral attachment. This delimitation is also visible in the sagittal view, and the pattern as seen on the 3D rendering corresponds to that observed in other species (e.g., *Canis*). Therefore, there is a clear continuity between the *nt* and the *sl*. The recess formed by the *sl* opens to form a ventrally oriented lamella, with a small recess in its ventralmost part. There is a short connection between this lamella and the putative *up*, which is located laterally to it. The main lamella then forms a dorsolateral recess, from which a new lamella emerges and that ends in contact with the cribriform plate. **Loxodonta**—We cannot confidently identify any *nt* or peculiar suture from the *sl*. When looking at the 3D rendering, an alternative interpretation could be that the identified maxilloturbinal (*mt*) is actually the *nt*. However, the ventral attachment of the main root of this large lamella argues for its recognition as a *mt* (see also supplementary figures in Martinez, Courcelle, et al., 2023; Martinez, Okrouhlik, et al., 2023). Therefore, we hypothesize the absence of a *nt* in *Loxodonta*. The potential *sl* is composed of two ventrally oriented lamellae that are attached together to a thick root. The most ventral part forms a recess, and then the lamellae split into numerous small lamellae, all of which originate from the same main lamella/root, so that we considered them as part of the *sl*. **Trichechus**—There is no clear delimitation between the potential *nt* and the *sl*. However, posteriorly there is a small delimitation with three lamellae of the *sl*. In the 3D rendering, a more anterior delimitation seems to be also present but it is not possible to separate the potential *nt* from the *sl*. In this species, we assume that the *nt* is present since it was clearly identified anterior to the semicircular lamina in young developmental stages (Genschow, 1934). Another unidentified lamella is also present dorsally to the potential *nt* + *sl* complex. This complex is an extremely thick and ovoid lamella oriented dorso-ventrally. Laterally, this large lamella reduces and transforms into three lamellae. The resulting three lamellae posteriorly fuse with the lateral wall of the nasal cavity close to the cribriform plate. These three lamellae may be considered as independent, but since they display a clear continuity with the potential *nt* + *sl* complex, we interpret them as *sl* (but see alternative delimitation in the 3D rendering). **Echinops**—The *nt* is a small ventrally oriented lamella with a thicker extremity on its ventral-most part that forms a very small recess. The *nt* classically reduces and ends with the development of the *sl*. On one side, a suture seems to indicate the separation between the *nt* and the *sl* slightly anterior to the usual delimitation when the *sl* opens into the large recess. In any case, the *sl* and *nt* show a clear continuity. The *sl* forms a large

recess with a dorsal and a lateral attachment. This recess opens in the nasal cavity, and the dorsal part separates from the ventro-lateral *up*. The dorsal part then forms a laterally scrolled lamella (as seen in most species) that ends at the level of the cribriform plate. Overall, the *sl* of *Echinops* presents a classical pattern, similar to that of other taxa such as *Mus. Galegeska*—The *nt* is composed of a small laterally scrolled lamella. The *nt* forms a small recess, then ends laterally. There is a large gap between the posterior end of the *nt* and the anterior part of the *sl*. The *sl* forms a short recess with two lateral attachments, then the recess opens and forms a long ventrally oriented lamella. This lamella delineates a large recess on its most ventral part, then forms a scrolled *sl* laterally that ends at the cribriform plate. **Orycteropus**—The *nt* consists of a long ventrally oriented lamella that ends where the *sl* forms a recess. As described in *Echinops*, a more anterior suture seems to indicate the limit between the *nt* and the *sl*. In any case, there is a clear continuity between the *nt* and the *sl*. The *sl* forms a large recess. One attachment migrates medially in contact with the nasal septum, while the other one migrates ventro-laterally. The enormous recess formed by the *sl* fuses with a third lamella that attaches dorsally. This dorsal lamella fuses with the medial lamella and several additional lamellae are formed on it. In the absence of a clear delimitation and as in other species (e.g., *Loxodonta*), these additional lamellae are considered to be part of the *sl*. The ventral *up* is well developed and consists of a long, laterally scrolled lamella that forms a tapering recess posteriorly. **Bradypus**—The *nt* is composed of a ventrally oriented lamella that is progressively extended by the *sl* as it forms a recess. A clear delimitation between the *nt* and the *sl* is visible in the ventralmost lamella of the *sl*. Therefore, there is a clear continuity between the *nt* and the *sl*. The *sl* forms a recess with a dorsal and a lateral attachment. A long, ventrally oriented lamella emerges from this recess. As the recess opens, the lamella starts to form the usual, laterally oriented scroll but fuses with an additional dorsally located lamella. The entire structure forms a dorsal recess, but only the ventral part is interpreted as part of the *sl*. The dorsal part of this lamella is continuous with other lamellae that form posteriorly an interturbinal (*it*) and the frontoturbinal 1 (*ft1*). **Dasypus**—The *nt* consists of a lamella that scrolls laterally and that is progressively extended posteriorly by the *sl* as it creates a recess. There is a clear continuity between the *nt* and the *sl*. However, posteriorly, the main root of the *nt* is thick and may be attributed to another lamella. Posteriorly, there is also a clear suture between this lamella and the *sl*. However, to be consistent with other species where we cannot clearly see this suture (e.g., *Talpa*, *Tapirus*, *Bradypus*, *Echinops*, *Orycteropus*), we have segmented this lamella as part of the *sl*.

The *sl* forms a very large recess with one dorsal and one lateral attachment. This recess is in contact with a lateral lamella that fuses posteriorly with the horizontal lamina (*hl*). This recess then opens to form a ventro-lateral and a dorso-medial lamella. The ventro-lateral *up* is large and forms a bifid scroll before its posterior end. Several smaller lamellae are attached to the main dorso-medial lamella, and in the absence of a clear delimitation, and as in other species, these additional lamellae are considered part of the *sl*.

3.2.2 | Maxilloturbinal

Mus—The maxilloturbinal (*mt*) attaches laterally and forms a bifid scroll with one branch facing dorsally and one facing ventrally. As it progresses posteriorly, the *mt* shifts ventrally to form the nasolacrimal canal and then separates from the lamina infraconchalis. The medial part of the nasolacrimal canal was not considered as *mt* when it separated posteriorly from the main lamella. Then the single ventral lamella reduces and ends with the development of a single lamella. The suture between the *mt* and this ventral lamella is clear (see also supplementary figure 8 in Martinez, Courcelle, et al., 2023; Martinez, Okrouhlik, et al., 2023). **Oryctolagus**—In this species, the *mt* is highly complex with a main branch from which numerous small lamellae originate. This main lamella is placed all along the lateral wall of the nasal cavity with a visible suture, which defines the nasolacrimal canal. The main lamella then clearly separates from the lamina infraconchalis. Here, the small numerous lamellae have merged into a thicker bony structure with some empty cavities in it. Then, as in *Mus*, the *mt* decreases with the development of the ventral lamella. A clear delimitation is visible in between. **Tupaia**—The *mt* is a complex bifid scroll shape with numerous additional lamellae on it. The main root lamella classically migrates from lateral wall of the nasal cavity to the ventral floor. The *mt* ends ventrally without any contact with the ventral lamella, which starts more posteriorly. **Galeopterus**—The *mt* is a small, ventrally scrolled lamella that migrates from lateral to ventral position and extends extremely far posteriorly. A clear delimitation between the *mt* and the ventral lamella is visible on one side of the specimen. **Homo**—The *mt* is a ventrally scrolled lamella that remains laterally attached until its posterior end. The delimitation is straightforward. The scrolled *mt* displays some small internal cavities. **Talpa**—The *mt* forms a bifid scroll with very few additional lamellae on it. It classically attaches laterally, migrates ventrally, and then reduces. We did not identify a clear suture between the *mt* and the ventral lamella, but the reduction of the *mt* is clear. **Erinaceus**—The *mt* is a complex structure where three main lamellae originate

from the main root lamella and numerous additional lamellae emerged from it. The main branch classically migrates from a lateral insertion to a ventral one and ends without contact with the ventral lamella. **Carollia**—The *mt* is a single ventrally oriented scrolled lamella, which migrates laterally to ventrally, but very medially when compared to other species. The *mt* seems to be progressively extended by the ventral lamella, but the exact boundary between the two structures is difficult to delineate. **Canis**—The *mt* is a highly complex and developed structure in this species. It is composed of a main lamella that scrolls ventrally, and numerous additional lamellae branch off all along this lamella. There is no continuity between the *mt* and the ventral lamella. **Manis**—The *mt* is a bifid scrolled lamella in which each scroll wraps around itself twice. A slight suture is visible during the *mt* and the ventral lamella. **Tapirus**—The *mt* of the *Tapirus* is an extremely large structure but not really complex. Anteriorly, the *mt* forms an open recess, then a very thick lamella migrates from the *mt* ventro-dorsally. An extremely large recess is shaped more posteriorly; it occupies most of the nasal cavity. From this recess, some smaller lamellae take root. The dorsal part of the main recess is extended by a second recess dorsally formed. This dorsal recess closes, as well as the main recess, more posteriorly. Posteriorly, there is no continuity between the *mt* and any other lamella. **Lama**—The *mt* is a bifid scrolled lamella in which each scroll wraps around itself twice (as in *Manis*). There is no continuity between the *mt* and the ventral lamella. **Procapra**—The *mt* starts with a dorso-ventral lamella that is curved. It then forms a bifid scroll lamella. Posteriorly, there is a clear suture between the *mt* and the ventral lamella. **Loxodonta**—The *mt* starts as a small lamella that quickly forms a recess with the lateral wall of the nasal cavity, then it reduces to a small lamella. Its posterior limit is easy to distinguish as there is no contact with additional lamellae. **Trichechus**—We could not identify a *mt*. Such an absence of *mt* was previously described (Genschow, 1934). **Echinops**—The *mt* is a well-developed ventrally scrolled lamella. A delimitation between the *mt* and the ventral lamella is visible. **Galegeska**—The *mt* is a bifid scrolled lamella that migrates from the lateral wall of the nasal cavity to the ventral floor of the nasal cavity. A suture is slightly visible between the *mt* and the ventral lamella. **Orycteropus**—The *mt* is a bifid scrolled lamella in which each scroll makes two full turns. A suture is slightly visible between the *mt* and the ventral lamella. **Bradypus**—Anteriorly, the *mt* is a bifid scrolled lamella. It then splits into two parts, a single scrolled lamella oriented dorsally and a long ventrally oriented lamella. Both parts end without any contact with additional lamellae. **Dasybus**—The *mt* is a bifid scrolled lamella. A suture is slightly visible between the *mt* and the ventral lamella.

3.2.3 | Frontoturbinals and interturbinals

Mus—It consists of the usual, single frontoturbinal 1 (*ft1*), which forms a bifid scroll. **Oryctolagus**—Both a bifid scrolled *ft1* and a simple, scrolled *ft2* are found. **Tupaia**—A bifid scrolled *ft1* and a single scrolled *ft2* are found. **Galeopterus**—It features *ft1* and *ft2*, are simple in shape, but form a very large recess, similar to all the other olfactory turbinals of the species. **Homo**—No *fts* have been identified. **Talpa**—Both *ft1* and *ft2* are present with bifid scrolls, with just one or two additional lamellae on them. **Erinaceus**—Both *ft1* and *ft2* are present with bifid scrolls, with only one additional lamella on them. **Carollia**—There is only one *ft1* that originates at the end of the *ls*. The *ft1* is ventrally scrolled and migrates dorso-medially, ending at the cribriform plate. **Canis**—We identified eight *fts*, including four *its*. The most ventral *ft* may have been identified as an *it* (Wagner & Ruf, 2019). However, to be consistent with the attribution made in other species, we considered it here to be a *ft*. Even though it did not reach the most medial part due to the packing with all the other *ft* and the *et*, this *ft* is very well developed. The four well developed *fts* form bifid scrolled turbinals. The most ventral *ft* and *it* are clearly attached to the horizontal lamina (*hl*) on a short distance. **Manis**—We identified eight *fts*, including three *its*. Four *fts* form bifid scrolled turbinals. Two *its* are extremely small. The three most ventral *fts* are in contact with the *hl* at one point. **Tapirus**—We identified 18 to 21 *fts*, including 13 to 16 *its*. Three *its* are extremely small. To be consistent with other species (except *Canis*, see above), we identified the *ft1* as a frontoturbinal; however, due to its particularly medial location, it may have been considered as *it* by other authors (see *Canis* and Wagner & Ruf, 2019). As with all the other olfactory turbinals in the species, the *fts* are highly developed and complex structures composed of multiple small lamellae. As the *fts* starts to decrease in size posteriorly, many additional *its* start to develop. **Lama**—We identified 10 *fts*, including 6 *its*. However, the attribution of “*it*” might be arbitrary for some turbinals. All the 10 *fts* present a unique pattern in forming large recesses. The exact delimitation is extremely complicated to assess since the roots of the turbinals fuse with various supporting lamellae in some areas (that are generally not considered as turbinals, e.g., *hl*). Interestingly, one of the frontoturbinals starts extremely anteriorly where the *mt* and *nt* are located. To our knowledge, this has never been reported in any taxon. Therefore, we may question the correct attribution to the “*ft*.” However, the attribution to “*ft*” is clearer posteriorly, and there is clear continuity with an absence of suture with the anterior part. **Procapra**—We identified a *ft1* as well as a potential *it*. This potential *it* forms a very

small recess on a few slices then fuses with the *hl*. ***Loxodonta***—We identified 34 *fts*, including 30 *its*. Five out of the 30 *its* are large and may be attributed to *fts*. Even more than with the ethmoturbinals (*ets*, see below), it is almost impossible to provide an exact count, since various lamellae fuse to different points. ***Trichechus***—If we consider the three lamellae that fuse with the *nt* + *sl* complex as *sl*, then we cannot identify any *ft* in this species. ***Echinops***—There are two *fts* and no *its*. Both *fts* are bifid, scrolled lamellae. ***Galegeeska***—There are two *fts* and no *its*. The *ft1* is a bifid, scrolled lamella and the *ft2* is a ventrally scrolled lamella. ***Orycteropus***—We identified 32 *fts*, including 21 *its*. In contrast to *Loxodonta* and *Tapirus*, the turbinals are much more intertwined with one another. It is very difficult to provide an exact count since many lamellae fuse on various points, but it is easier than in *Loxodonta*. ***Bradypus***—There are four *fts*, including two *its*. The *ft1* is a very long lamella with a dorsal scroll. The long roots of the *ft1* attach and fuse with some part of the *sl*, which makes the precise delimitation difficult. ***Dasyus***—There are 16 *fts*, including 10 *its*. As in *Orycteropus*, the *fts* are really intertwined with one another. The attribution to one *ft* or *it* is mostly based on the 3D rendering.

3.2.4 | The ethmoturbinal I

Mus—It features the usual ethmoturbinal I (*etI*) in which the pars anterior (*pa*) and pars posterior (*pp*) are clearly discriminated; they are fused posteriorly. ***Oryctolagus***—The *pa* and *pp* are only separated in a small area in the middle. ***Tupaia***—The *etI* is extremely developed anteriorly and wraps around a part of the maxilloturbinal (*mt*). The *pa* and *pp* are separated anteriorly and fused posteriorly. ***Galeopterus***—The *pa* and *pp* of the *etI* form large recesses anteriorly and are fused posteriorly. ***Homo*** The *etI* probably consists only of the pars anterior (see also Martinez, Amson, Ruf, et al., 2024). It is a dorsally attached ventrally directed lamella, with a small recess in its ventralmost part. Posteriorly it migrates more laterally. ***Talpa***—The *pa* starts very anteriorly where the *mt* and *nt* are still present. Posteriorly, the *pa* and *pp* form two lamellae that are scrolled ventrally and dorsally, respectively. The root of *pa* and *pp* seems to be always connected. Only the upper part is separated anteriorly. ***Erinaceus***—The *pa* starts relatively anteriorly where the *mt* and *nt* are still present. Posteriorly, the *pa* and *pp* form two lamellae with additional lamellae on them. The *pa* and *pp* are clearly separated anteriorly and then fused posteriorly. ***Carollia***—The *etI* is composed of a main lamella that connects two smaller lamellae. In this taxon, the *pa* and *pp* are always

connected. ***Canis***—The *etI* starts very anteriorly, where the *mt* and *nt* are located. In this anterior part, the *etI* is highly complex with numerous small lamellae. Posteriorly, a main branch is attached to several bifid, scrolled lamellae. The most ventral of these lamellae were considered by Wagner and Ruf (2019) to be an *it*. The distinction between the *pa* and *pp* is not as clear as in other species, and they seem to be connected along their entire length. ***Manis***—The *etI* starts anteriorly, forming a recess. The *etI pa* and *pp* are composed of a long lamella with numerous small lamellae attached to it. In the individual examined, the *pa* and *pp* are never in contact. However, based on the 3D rendering of other *Manis* species and of another individual of *Manis javanica* (MorphoSource media 000072148, USNM 198852), we hypothesize that these two major turbinals are *pa* and *pp* of the *etI* as was also hypothesized by Ito et al. (2023). In the other individual (USNM 198852), these two parts are almost in contact, and there is no apparent *it* in between them. In the individual sampled in this study, two *its* are present in between the *pa* and *pp*. ***Tapirus***—The *etI* is composed of two separate, long and thick lamellae (*pa* and *pp*) from which numerous additional smaller lamellae branch off. Based on the comparison of all other species studied and especially the two individuals of *Manis javanica*, we hypothesize that the two main segmented lamellae are *pa* and *pp* of the *etI*. Five *its* are located between these two pars. ***Lama***—Anteriorly, the *etI* forms a large recess where the *mt* and *nt* are present. Posteriorly, it presents numerous smaller recesses, and displays a more commonly observed morphology. The root of the identified *pp* is always in contact with the root of the *pa*. Anteriorly, a recess in contact with the *pp* has been interpreted as an *it*, since it is clearly posteriorly extended by the *pp*. However, it may also have been identified as part of the *pp*. ***Procapra***—The *etI* forms a recess anteriorly. Posteriorly, it forms a main lamella that subdivides into two lamellae scrolled ventrally and dorsally, respectively. The *pa* and *pp* are always connected through to lamellae. ***Loxodonta***—As in *Tapirus* and *Manis*, even if the *pa* and *pp* are always separated, we identified them as the *etI*. Between the *pa* and *pp*, we identified two well-developed *its* and six smaller ones (mostly located posteriorly). ***Trichechus***—The *etI* is a thick lamella with a very thick circular shape. We could not distinguish two parts, so we hypothesized that the *etI* is not bipartite. ***Echinops***—The *etI* is composed of two main lamellae with bifid, scrolled lamellae at its extremity. The *pa* and *pp* are separated anteriorly and fused posteriorly. ***Galegeeska***—The *etI* starts anteriorly by forming a recess. The *pa* and *pp* are separated anteriorly for a short distance and fused posteriorly. ***Orycteropus***—The *etI* is highly developed. When examining the medial view of the 3D

rendering, it appears as if additional ethmoturbinals have not been separated from the volume identified as *etI*. However, based on this adult individual, such segmentation appears to be accurate. Indeed, all the subunits fused at one point, a pattern that is consistent with how this turbinal was segmented in the other species. Three to four major branches that fuse anteriorly appear to correspond to the area where all the other lamellae originate from, as seen on the 3D rendering. Only the most posterior part of these three to four main roots may be separated as another ethmoturbinal (see dark gray color labeled as “unidentified lamella”). Further posteriorly, however, some small lamellae fuse together, so that it is no longer possible to delimitate them with precision. In this species, the *pa* from the *pp* cannot be delimited with confidence, ditto for some interturbinals located in between the *etI*, as observed in other species showing a large number of turbinals. **Bradypus**—The *etI* starts anteriorly by forming a recess. The roots of the *pa* and *pp* are always in contact. **Dasyus**—The posterior delimitation of the *etI* is extremely difficult and should involve sampling additional adult individuals. A first hypothesis is figured in Figure 13. However, based on the 3D rendering, a second hypothesis might be to include the posteriorly located, well-developed turbinal to the *etI* (see dark gray color labeled as “unidentified lamella” in Figure 13). Indeed, as in *Orycteropus*, a main branch of these lamellae seems to extend in the direction of the rest of the *etI*. However, unlike *Orycteropus*, the end of this lamella does not go directly to the *etI* and fuse with it. One to two very small *its* that are located medially may be considered as located in between the different pars of the *etI*.

3.2.5 | Ethmoturbinals and interturbinals

—**Mus**—Four ethmoturbinals (*ets*), including the “main” interturbinal (*main it*), are present. **Oryctolagus**—Three to four *ets*, including a greatly reduced *main it* (barely visible) are present. **Tupaia**—Four *ets* (including the *main it*) are present. The ethmoturbinal II (*etII*) is composed of a main lamella, laterally scrolled, with a bifid scrolled lamella that attaches on the main lamella. These two parts may in some respects look like two distinct turbinals (but see Ruf, 2014). The ethmoturbinal III (*etIII*) is composed of the scrolled lamella that is almost entirely attached to the *etII* (see also Ruf, 2014). **Galeopterus**—Five *ets* (including the *main it*) are present. All turbinals display a unique morphology that forms a large recess. The *etII* and *etIII* were considered independently since they are in contact only in a few slices thanks to the presence of a small lamella that may not be considered as a turbinal. As a result, the most

ventro-posterior turbinal is identified as *etIV*. However, if we follow the way the *ets* of *Tupaia* were identified, then the *etII* and *etIII* of *Galeopterus* could represent two parts of the *etII*. **Homo**—Apart from the *etI pa*, *Homo* has only one *etII*, which is a short but relatively thick lamella that is dorsally attached and migrates slightly laterally proceeding posteriorly. **Talpa**—Four *ets* (including the *main it*) are present. The *etII* presents the same pattern as *Tupaia* with a bifid scroll shape always connected to the other lamella. **Erinaceus**—It presents a total of four *ets* including the *main it*. The *etII* resembles the pattern observed in *Tupaia* and *Talpa*. **Carollia**—Four *ets* (including the *main it*) are present. **Canis**—Four *ets*, including the *main it* and one additional *it*, are present. The *etII* starts very anteriorly. Posteriorly, the *etII* resembles that of *Tupaia*, *Talpa*, and *Erinaceus* characterized by a bifid scrolled lamella attached to the main turbinal and a few additional lamellae. **Manis**—Nine *ets*, including the *main it* and three additional *its*, are present. Posteriorly, the *etII* resembles that of *Tupaia*, *Talpa*, *Erinaceus* and *Canis*. **Tapirus**—A total of 23 to 25 *ets*, including the *main it* and 17 to 19 additional *its*, are present. Among the 19 *its*, two are very small and hardly visible. For some large *its*, it remains difficult to identify them as either *it* or *et*. **Lama**—Eight to ten *ets*, including the *main it* and three to five additional *its*, are present. Two of the *its* are very small and barely visible. All the *ets*, except the two barely visible *its*, form a recess. The most ventro-posterior turbinal is identified as an *et*, but since it is very small, it could also be an *it*. **Procvavia**—Four *ets* (including the *main it*) are present. **Loxodonta**—We identified 19 *ets* including the *main it* and 15 additional *its*. This results in a relatively low number of *ets* (only *etI*, *etII*, and *etIII*) compared to that of the *its*. The exact number is difficult to estimate since some *its* are fused or connected to additional lamellae over a short distance. **Trichechus**—This genus presents a total of four *ets* including the *main it*. All of these *ets* are extremely thick except the *etII*. The *etIII* forms a long lamella located very anteriorly, then decreases in length to finally thicken posteriorly and form a very thick lamella. **Echinops**—Four *ets* (including the *main it*) are present. The *etII* is similar to other species with a main lamella and a bifid scrolled lamella on it. **Galegeeska**—Four *ets* (including the *main it*) are present. The *etII* is similar to other species with a main lamella and a bifid scrolled lamella on it. **Orycteropus**—We identified 14 *ets* including the *main it* and 8 additional *its*. As with the *ets*, the attribution of the *its* is mostly based on the 3D rendering. The most posterior *ets* are very intertwined, both with each other and with the other *ets*. **Bradypus**—A total of 12 *ets*, including the *main it* and six additional *its*, are present.

Dasypus—We identified 22 *ets*, including the *main it* and 12 additional *its*. The exact delimitation and attribution of some *its* is difficult because they are connected to some *ets*. Some *ets* are highly intertwined with one another, and the *its* were mostly identified based on the 3D rendering.

3.2.6 | The “main” interturbinal

Mus—The “main” interturbinal (*main it*) presents a simple dorsally scrolled lamella. **Oryctolagus**—Almost absent on one side and very slightly visible on the other side. May also be considered absent (see also Ruf, 2014). **Tupaia**—It forms a bifid scroll. **Galeopterus**—The *main it* forms a large recess that opens posteriorly. **Homo**—No *main it* identified. **Talpa**—A single, dorsally scrolled *main it* is present. **Erinaceus**—A small, dorsally scrolled *main it*. **Carollia**—A dorsally scrolled *main it* with a small recess on its upper part. **Canis**—A ventrally scrolled lamella that is anteriorly attached to the *etII*. **Manis**—A small bifid scrolled lamella. **Tapirus**—The *main it* is composed of a main lamella with additional lamellae branching on it. We identified two smaller *its* dorsally located to this larger *it*; however, we hypothesize that this larger interturbinal is the *main it*. **Lama**—A small lamella shaping a recess. **Procavia**—A rather developed *main it* that forms a large recess. **Loxodonta**—The potential *main it* is between two other smaller *its*. **Trichechus**—This is a very thick and short *main it* that attaches directly onto the lateral wall of the nasal cavity. It does not really extend to form a lamella. **Echinops**—The interturbinal starts as a bifid scrolled lamella originating from the *etII*, then it separates from it and forms a dorsal scrolled lamella. **Galegeska**—The *main it* is a dorsally scrolled lamella. **Orycteropus**—Due to the uniqueness of the *etI* (see above), it is difficult to ascertain the *main it*. Here, we identified the *main it* as the first turbinal located ventrally to the identified *etI*. **Bradypus**—The *main it* is a dorsally scrolled lamella. **Dasypus**—We identified the *main it* as the first turbinal located ventrally to the identified *etI*. However, since the posterior delimitation of the *etI* is unclear (see above), the identification of the *main it* remains uncertain.

4 | DISCUSSION

4.1 | Morphological disparity across species

As previously documented, the disparity of turbinals across tetrapods is considerable (Bang, 1971; Martinez,

Amson, Ruf, et al., 2024; Negus, 1958; Parsons, 1967; Paulli, 1900a; Paulli, 1900b; Paulli, 1900c). In placental mammals, this disparity is manifested by variations in the number, size, shape, complexity, and thickness of turbinals (Figures 1 and 2).

4.1.1 | Number

The turbinal count varies widely, from zero in *Pontoporia* to approximately 110 in *Loxodonta* (considering both right and left sides). With the coarse sampling used here, considering one species per order, it appears that the number of turbinals may be partially related to body size (Figures 1 and 2). However, some species deviate from this, such as *Homo*, *Pontoporia*, and *Trichechus*, which have relatively few turbinals despite their large body size (Figures 1, 2, 5, and 10), and which is likely due to ecological factors such as aquatic lifestyles for the latter two. Indeed, the reduction (and in some cases loss) of the number of turbinals is well documented in the evolutionary history of cetaceans (Berta et al., 2014; Farnkopf et al., 2022; Godfrey et al., 2013; Ichishima, 2016; Peri et al., 2020). This is likely associated with the modification of the respiratory system and the difficulty in detecting odorants underwater. In rodents, it has been demonstrated that the semi-aquatic coypu (nutria, *Myocastor coypus*) has lost two olfactory turbinals and gained one respiratory turbinal in comparison to its close terrestrial relative, the Guyenne spiny-rat (*Proechimys guyanensis*; Martinez et al., 2020).

The reduction of the number of turbinals is documented in other mammalian clades. In the subterranean naked mole-rat (*Heterocephalus glaber*), a highly reduced or even loss of maxilloturbinal (in some individuals) cannot be solely attributed to the subterranean lifestyle, as the closely related subterranean Mashona mole-rat (*Fukomys darlingi*) presents a fully grown maxilloturbinal (Martinez, Okrouhlik, et al., 2023). In primates, turbinal loss and gain convergently occur in different clades, but the explanation behind it remains elusive. (Lundeen & Kirk, 2019; Smith et al., 2014, 2016). Some hypotheses discuss the potential impact of the lack of an olfactory recess in certain groups, the midfacial and nose morphology, the developmental patterns related to respiration and airflow dynamics, and finally some potential sensory trade-offs between vision and olfaction (Lundeen & Kirk, 2019; Niimura et al., 2018; Smith et al., 2014, 2016). Conversely, the presence of numerous turbinals is not functionally understood. For instance, the investigated *Dasypus* feature approximately 82 turbinals (see Figures 2, 13, and 14), which cannot be simply ascribed to an effect of size given that it is rather intermediate among

the full range of mammalian body sizes. Intraspecific and intraindividual variation in the turbinal count was described in various orders (Lundeen & Kirk, 2019; Macrini, 2012; Martinez et al., 2018; Martinez, Amson, Ruf, et al., 2024; Martinez, Okrouhlik, et al., 2023; Rowe et al., 2005; Ruf, 2014, 2020; Smith & Rossie, 2006). As an example, humans who generally have three turbinals, may present a fourth one, and exceptionally, five (on one side; Rusu et al., 2019).

While a phylogenetic trend in the turbinal number is evident within some mammalian orders, with a relatively constant number of turbinals within a mammalian order (Macrini, 2012; Martinez et al., 2018, 2020; Ruf, 2014), notable exceptions exist, such as the discrepancy between *Loxodonta* and *Procapra* (Figures 9 and 10) that may also be attributed to size in this example. However, statistical analyses to investigate the turbinal scaling in a phylogenetically informed context are pending. The maximum number of about 110 turbinals identified in *Loxodonta* (Figures 10 and 14) contrasts sharply with Paulli's earlier identification of about 52 olfactory turbinals in *Loxodonta* (Paulli, 1900b). Several factors may explain such differences in turbinal counts. First, Paulli did not have access to 3D virtual data, making it challenging to discriminate highly intricate structures such as the olfactory turbinals of *Loxodonta*. Additionally, the specimen Paulli studied was young (“*eines jüngerer Exemplars*”; Paulli, 1900b, p. 235); additional lamellae could develop during ontogeny (e.g., Smith et al., 2023). Furthermore, based on the available schematic drawing, it appears that Paulli interpreted as bony struts of the pneumaticity of the skull what we identified as potential turbinals. Our identification is based on clear differences, such as variations in thickness between turbinals and these bony struts, with the latter typically being the thicker of the two (Supplementary Figure 1). This example underscores the challenge of accurately counting turbinals, especially in species with high complexity or number, where fusion of small interturbinals and lamellae complicates attribution (Figure 14). Moreover, applying the common definition of interturbinals as turbinals that do not extend as medially as others (Martinez, Amson, Ruf, et al., 2024) is extremely challenging in species with a high number of turbinals and/or complex turbinals. We observed significant differences in the challenges faced when delimiting turbinals in *Loxodonta* compared to *Dasyopus* or *Orycteropus*. In the latter two species, main branches connect the small turbinal lamellae, which makes it easier to consistently define individual turbinals. However, in *Loxodonta*, attributing interturbinals to a single structure is extremely difficult due to various fusions with different lamellae that are not turbinals, especially for the most posterior ones. Similarly, in species with complex,

numerous turbinals, such as *Manis*, *Tapirus*, *Loxodonta*, *Orycteropus*, and *Dasyopus*, delimiting some turbinals is complicated, making it challenging to resolve homology across species (Figure 14). The consideration of multiple developmental stages is critical to overcome these challenges (Ito et al., 2021, 2022; Macrini, 2014; Macrini et al., 2023; Ruf, 2020; Smith et al., 2023). However, including multiple species within a given mammalian order, as well as across different mammalian orders also facilitates the process of establishing homology. In this study, having a clear understanding of homology associated with the morphology of well-known orders aided in identifying and characterizing turbinals in other orders. Therefore, having access to smaller species in orders with a large size range should help clarify turbinate homology of larger species (e.g., within Artiodactyla) in the future.

4.1.2 | Relative size

The relative size of turbinals should be assessed using quantitative data on their surface area, skull length, body mass, or nasal cavity volume. Although this was not done here, it is clear that turbinal occupancy relative to the overall skull volume differs across species, with for example turbinals appearing highly reduced in *Homo* and densely packed in *Orycteropus* (Figures 1, 5, and 12). Quantitative data could help to confirm the precise relationship between density of packing and relative turbinal size.

4.1.3 | Shape and complexity

Turbinal shape varies widely, with most variation attributed to the maxilloturbinal, nasoturbinal, and semicircular lamina. The maxilloturbinal, in particular, exhibits changes that follow the shape of the nasal cavity (Martinez, Okrouhlik, et al., 2023). Some species show turbinals forming large recesses or multiple small ones, while *Galeopterus* and *Lama* display almost all turbinals forming large recesses (Figures 4 and 9). The pattern of the *Lama* is unique, with all turbinals forming recesses that occupy almost all nasal cavity space, leaving little space between them (Figures 9). In this study, we demonstrated that certain species exhibit high turbinal complexity as well as intricate olfactory turbinals with minimal spacing between them, such as *Canis*, *Tapirus*, *Manis*, *Lama*, and *Tapirus* (Figures 7, 8, and 9). Moreover, species like *Loxodonta*, *Orycteropus*, and *Dasyopus* represent extreme examples of turbinal complexity (Figures 10, 12, and 13). Our sampling suggests that increased complexity tends to correlate with both the size and number of

turbinals. *Bradypus* stands out as an exception, with a relatively high number of simple-shaped turbinals (Figure 12). On a finer scale, especially in rodents, the complexity of turbinal bones can vary significantly in species with the same number of turbinals. In such cases, the evolution of complexity has been linked to dietary specialization (Martinez et al., 2018). While the highly specialized myrmecophagous diet of *Orycteropus* (Taylor et al., 2002) may align with this pattern observed in rodents, it does not necessarily apply to *Dasybus novemcinctus*, which has a more generalized diet (Redford, 1986). Nonetheless, further quantitative analyses are pending, such as phylogenetic comparative analyses based on the surface area of turbinals.

4.1.4 | Thickness of turbinal bones

Variation in turbinal thickness exists between species. It is relatively common for certain areas to exhibit greater thickness. For instance, a small portion of the pars anterior of ethmoturbinal I is significantly thicker in *Oryctolagus* and *Echinops* (Figures 11 and 12). *Erinaceus*, on the other hand, appears to have slightly thicker turbinals overall, with some intraspecific variation observed. In this species, the ventral portion of the semicircular lamina is particularly thick (Figure 6). Additionally, *Bradypus* shows a slight overall increase in thickness, especially in the upper part of most of the turbinals (Figure 12). Notably, almost all turbinals of *Trichechus* exhibit exceptional thickness (Figure 10), likely attributed to a potential systemic increase in bone mass (Amson et al., 2018). Other intraspecific variations in turbinal thickness have been previously mentioned in species such as humans (Marks et al., 2019).

4.2 | Olfactory turbinals and the challenge for quantitative approaches

In some mammalian orders, particularly among small to medium-sized species where the number and epithelial cover of turbinals are well understood, accurate delineation between respiratory and olfactory turbinals may be used in quantitative analyses (Martinez et al., 2018, 2020; Martinez, Courcelle, et al., 2023; Martinez, Okrouhlik, et al., 2023; Yohe et al., 2022). At the scale of placental mammals, however, this task becomes more challenging. First, in some species, the posterior part of the nasoturbinal is known to be covered by olfactory epithelium (Martinez, Amson, Ruf, et al., 2024; Smith et al., 2004, 2012; Smith & Rossie, 2008; Yee et al., 2016). Moreover, the exact limit between the nasoturbinal and semicircular

lamina is difficult to delineate in some species, further complicating the issue. Furthermore, in some species, the anterior part of the ethmoturbinal I is covered by respiratory epithelium, further complicating the delimitation process (Martinez et al., 2020; Martinez, Amson, Ruf, et al., 2024; Pang et al., 2016; Smith et al., 2016; Smith, Bhatnagar, et al., 2007; Yee et al., 2016). In some species, this portion covered by respiratory epithelium may represent a significant portion of the ethmoturbinal I. For example, that of *Galeopterus* extends far anteriorly with the naso and maxilloturbinal (Figure 4). This difficulty highlights the importance of histological investigations; however, obtaining histological sections from large adult individuals is challenging. Another approach to address this olfactory-respiratory delimitation may be through diceCT imaging (Martinez, Amson, Ruf, et al., 2024; Smith et al., 2022; Smith, Corbin, et al., 2021; Smith, Craven, et al., 2021; Yohe et al., 2022). However, staining large adult mammal heads for this purpose also poses practical challenges. In the absence of an ideal method, one approach for quantitative analysis may be to make an antero-posterior delineation of all the turbinals from the anterior portion of the semicircular lamina. The olfactory part would include the posterior part of this delineation but exclude the maxilloturbinal in full. Conversely, the respiratory part would include both the anterior part of this delineation and the maxilloturbinal. However, such an antero-posterior delineation lacks precision and may not provide detailed comparative data, allowing only for the interpretation of general trends and large differences. In focusing on the heat and moisture conservation aspect of the turbinals, Martinez, Courcelle, et al. (2023) and Martinez, Okrouhlik, et al. (2023) chose to include only the maxilloturbinal where the epithelial cover is clear and after demonstrating a significant relationship between the surface area of the nasoturbinal and maxilloturbinal as well as the absence of trade-off between them.

Regarding the number of olfactory turbinals, there is a relationship between the number of these turbinals and the number of functional olfactory receptor genes at a broad scale, which may be related to actual olfactory performance (Martinez, Amson, & Laska, 2024). This relationship, however, does not hold at finer taxonomic scales (Martinez, Amson, Ruf, et al., 2024; Martinez, Courcelle, et al., 2023). Consequently, we believe its significance to be limited compared to approaches focusing on the surface area of olfactory turbinals (Martinez et al., 2018, 2020; Martinez, Courcelle, et al., 2023; Van Valkenburgh et al., 2011; Yohe et al., 2022).

Given the challenge of precisely delineating the olfactory from the respiratory parts of some turbinals in certain mammalian species, and considering that the

number of olfactory turbinals may not serve as a precise proxy, one can question the notion that turbinals are the best proxy for studying olfaction from a morphological perspective. Another of such proxies is the olfactory bulb, the morphology of which can also be assessed on dry skulls through the segmentation of its endocast. However, this approach is not ideal either, since it is not possible to distinguish between the areas of the main olfactory bulb and the accessory olfactory bulb with such an endocast. This may however provide informative data for the overall chemosensory proxy (= related to the detection of chemical stimuli). Indeed, the main olfactory bulb is primarily associated with the centralization of olfactory information (mainly from the olfactory epithelium of the olfactory turbinals and the nasal cavity), while the accessory olfactory bulb receives vomero-olfactory information (mainly from the vomeronasal organ; Storan & Key, 2006). Therefore, in that sense, the epithelium of the olfactory turbinals presents more precise information about olfaction.

Overall, our investigation of turbinals across placental mammals underscores their remarkable diversity and evolutionary significance. We found substantial variation in turbinal number, size, and shape, indicating complex patterns of adaptation and phylogenetic history. Moreover, our study reveals challenges in turbinal nomenclature, highlighting the importance of developmental research for resolving homologies. The number, relative size and complexity of turbinals have been associated with structural or functional constraints in a few mammalian clades only, making the morphofunctional anatomy of turbinals a promising research avenue. By shedding light on the intricate morphology of turbinals, our work contributes to a deeper understanding of mammalian nasal anatomy and its evolutionary basis.

AUTHOR CONTRIBUTIONS

Quentin Martinez: Conceptualization; data curation; writing – original draft; writing – review and editing. **Mark Wright:** Data curation. **Benjamin Dubourguier:** Data curation. **Kai Ito:** Data curation. **Thomas van de Kamp:** Data curation. **Elias Hamann:** Data curation. **Marcus Zuber:** Data curation. **Gabriel Ferreira:** Data curation. **Rémi Blanc:** Data curation. **Pierre-Henri Fabre:** Data curation. **Lionel Hautier:** Data curation; writing – review and editing. **Eli Amson:** Conceptualization; data curation; writing – original draft; writing – review and editing.

ACKNOWLEDGMENTS

The authors thank all the MorphoSource contributors and especially the members of the Van Valkenburgh lab who made available high-quality CT-data for some big

mammalian species. The authors acknowledge the Synthesis of Systematic Resources (SYNTHESYS+) project, which is financed by European Community Research Infrastructure Action (GB-TAF-1316 to the National History Museum, London), the Alexander von Humboldt foundation (Q.M. FRA—1222365—HFST—P), the Agence Nationale de la Recherche (Défi des autres savoirs, Grants DS10, ANR-17-CE02-0005 RHINOGRAD 2017, PHF), and the Bundesministerium für Bildung und Forschung (BMBF; Project KI-Morph 05D2022) that funded this research. The authors thank R. P. Miguez and V. Fernandez who gave them access to some specimens and the CT-scan facilities. The authors also thank Renaud Lebrun and Guillaume Captier who gave them access to the CT-scan of the human head for another research article. This CT-data were performed using the CT facilities of the MRI platform member of the national infrastructure France-BioImaging supported by the French National Research Agency (Grant ANR-10-INBS-04, “Investments for the future”), and those of the Laboratoire d'Excellence Centre Méditerranéen de l'Environnement et de la Biodiversité (LabEx CeMEB, ANR10-LABX-0004). The authors thank S. Merker and C. Leidenroth who gave them access to the skulls of *Trichechus manatus* and *Pontoporia blainvillei* from the SMNS collections as well as Matthias Boller for his help with the latter. This research was supported by a European Research Council consolidator grant (ConvergeAnt; ERC-2015-CoG-683257, PI F. Delsuc) and grants from French National Research Agency (CEBA: ANR-10-LABX-25-01). This is a contribution of ISEM 2024-169. Open Access funding enabled and organized by Projekt DEAL.

ORCID

Quentin Martinez  <https://orcid.org/0000-0002-7127-4012>

Gabriel Ferreira  <https://orcid.org/0000-0003-1554-8346>

Lionel Hautier  <https://orcid.org/0000-0001-8701-5421>

Eli Amson  <https://orcid.org/0000-0003-1474-9613>

REFERENCES

- Amson, E., Billet, G., & de Muizon, C. (2018). Evolutionary adaptation to aquatic lifestyle in extinct sloths can lead to systemic alteration of bone structure. *Proceedings of the Royal Society B*, 285, 20180270.
- Bang, B. G. (1971). Functional anatomy of the olfactory system in 23 orders of birds. *Acta Anatomica*, 79, 1–76.
- Berta, A., Ekdale, E. G., & Cranford, T. W. (2014). Review of the cetacean nose: Form, function, and evolution. *The Anatomical Record*, 297, 2205–2215.
- Bhatnagar, K. P., & Kallen, F. C. (1974). Morphology of the nasal cavities and associated structures in *Artibeus jamaicensis* and *Myotis lucifugus*. *American Journal of Anatomy*, 139(2), 167–189.

- Billet, G., Hautier, L., de Thoisy, B., & Delsuc, F. (2017). The hidden anatomy of paranasal sinuses reveals biogeographically distinct morphotypes in the nine-banded armadillo (*Dasyus novemcinctus*). *PeerJ*, 5, e3593.
- Bouckaert, R., Heled, J., Kühnert, D., Vaughan, T., Wu, C.-H., Xie, D., Suchard, M. A., Rambaut, A., & Drummond, A. J. (2014). BEAST 2: A software platform for Bayesian evolutionary analysis. *PLOS Computational Biology*, 10, e1003537.
- Collins, J. C., Pilkington, T. C., & Schmidt-Nielsen, K. (1971). A model of respiratory heat transfer in a small mammal. *Biophysical Journal*, 11, 886–914.
- Evans, C. (2003). *Vomer nasal chemoreception in vertebrates: A study of the second nose*. Imperial College Press.
- Farnkopf, I. C., George, J. C., Kishida, T., Hillmann, D. J., Suydam, R. S., & Thewissen, J. G. M. (2022). Olfactory epithelium and ontogeny of the nasal chambers in the bowhead whale (*Balaena mysticetus*). *The Anatomical Record*, 305, 643–667.
- Fawcett, E. (1921). The primordial cranium of *Tatusia novemcincta* as determined by sections and models of the embryos of 12 millimetre and 17 millimetre C.R. length. *Journal of Anatomy*, 55, 187–219.
- Fischer, E. (1901). Das Primordialcranium von *Talpa europaea*: Ein Beitrag zur Morphologie des Säugetierschädels. *Anatomische Hefte*, 17, 468–548.
- Ganeshina, L. V., Vorontsov, N. N., & Chabovsky, V. I. (1957). Comparative morphological study of the nasal cavity structure in certain representatives of the order Insectivora. *Zoologicheskii Zhurnal*, 36, 122–138.
- Genschow, J. (1934). Über den bau und die entwicklung des geruchsorgans der Sirenen. *Zeitschrift für Morphologie und Ökologie der Tiere*, 28, 402–444.
- Giannini, N. P., Macrini, T. E., Wible, J. R., Rowe, T. B., & Simmons, N. B. (2012). The internal nasal skeleton of the bat *Pteropus lylei* K. Andersen, 1908 (Chiroptera: Pteropodidae). *Carnegie Museum of Natural History*, 81, 1–17.
- Godfrey, S. J., Geisler, J., & Fitzgerald, E. M. G. (2013). On the olfactory anatomy in an archaic whale (Protocetidae, Cetacea) and the Minke whale *Balaenoptera acutorostrata* (Balaenopteridae, Cetacea). *The Anatomical Record*, 296, 257–272.
- Green, P. A., Valkenburgh, B., Pang, B., Bird, D., Rowe, T., & Curtis, A. (2012). Respiratory and olfactory turbinal size in canid and arctoid carnivorans. *Journal of Anatomy*, 221, 609–621.
- Ichishima, H. (2016). The ethmoid and presphenoid of cetaceans. *Journal of Morphology*, 277, 1661–1674.
- Ito, K., Kodeara, R., Koyasu, K., Martinez, Q., & Koyabu, D. (2022). The development of nasal turbinal morphology of moles and shrews. *Vertebrate Zoology*, 72, 857–881.
- Ito, K., Kodera, R., Noriyuki, K., & Kubo, M. (2023). On the development of the nasal turbinals and homology in laurasiatherians, with special reference to pangolins. *International Congress of Vertebrate Morphology (ICVM), Cairns, Australia*, 43–48.
- Ito, K., Tu, V. T., Eiting, T. P., Nojiri, T., & Koyabu, D. (2021). On the embryonic development of the nasal turbinals and their homology in bats. *Frontiers in Cell and Developmental Biology*, 9, 379.
- Jackson, D. C., & Schmidt-Nielsen, K. (1964). Countercurrent heat exchange in the respiratory passages. *Proceedings of the National Academy of Sciences of the United States of America*, 51, 1192–1197.
- Lovegrove, B. G. (2012). The evolution of endothermy in Cenozoic mammals: A plesiomorphic-apomorphic continuum. *Biological Reviews*, 87, 128–162.
- Lundeen, I. K., & Kirk, E. C. (2019). Internal nasal morphology of the Eocene primate *Rooneyia viejaensis* and extant Euarchonta: Using μ CT scan data to understand and infer patterns of nasal fossa evolution in primates. *Journal of Human Evolution*, 132, 137–173.
- Macrini, T. (2012). Comparative morphology of the internal nasal skeleton of adult marsupials based on X-ray computed tomography. *Bulletin of the American Museum of Natural History*, 365, 1–91.
- Macrini, T. E. (2014). Development of the ethmoid in *Caluromys philander* (Didelphidae, Marsupialia) with a discussion on the homology of the turbinal elements in marsupials. *The Anatomical Record*, 297, 2007–2017.
- Macrini, T. E., Hopwood, J., Herbert, C. A., & Weisbecker, V. (2023). Development of the ethmoid in a wallaby and implications for the homology of turbinal elements in marsupials. *Philosophical Transactions of the Royal Society B: Biological Sciences*, 378, 20220082.
- Maier, W. (1993). Cranial morphology of the therian common ancestor, as suggested by the adaptations of neonate marsupials. In F. S. Szalay, M. J. Novacek, & M. C. McKenna (Eds.), *Mammal phylogeny: Mesozoic differentiation, multituberculates, monotremes, early therians, and marsupials* (pp. 165–181). Springer.
- Maier, W., & Ruf, I. (2014). Morphology of the nasal capsule of primates—With special reference to *Daubentonia* and *Homo*. *Anatomical Record*, 297, 1985–2006.
- Marks, T. N., Maddux, S. D., Butaric, L. N., & Franciscus, R. G. (2019). Climatic adaptation in human inferior nasal turbinate morphology: Evidence from Arctic and equatorial populations. *American Journal of Physical Anthropology*, 169, 498–512.
- Martinez, Q., Amson, E., & Laska, M. (2024). Does the number of functional olfactory receptor genes predict olfactory sensitivity and discrimination performance in mammals? *Journal of Evolutionary Biology*, 37, 238–247.
- Martinez, Q., Amson, E., Ruf, I., Smith, T. D., Pirot, N., Broyon, M., Lebrun, R., Captier, G., Martín, C. G., Ferreira, G. S., & Fabre, P.-H. (2024). Turbinal bones are still one of the last frontiers of the tetrapod skull: Hypotheses, challenges and perspectives. *Biological Reviews*, 99(6). <https://doi.org/10.1111/brv.13122>
- Martinez, Q., Clavel, J., Esselstyn, J. A., Achmadi, A. S., Grohé, C., Pirot, N., & Fabre, P.-H. (2020). Convergent evolution of olfactory and thermoregulatory capacities in small amphibious mammals. *PNAS*, 117, 8958–8965.
- Martinez, Q., Courcelle, M., Douzery, E., & Fabre, P.-H. (2023). When morphology does not fit the genomes: The case of rodent olfaction. *Biology Letters*, 19, 20230080.
- Martinez, Q., Lebrun, R., Achmadi, A. S., Esselstyn, J. A., Evans, A. R., Heaney, L. R., Miguez, R. P., Rowe, K. C., & Fabre, P.-H. (2018). Convergent evolution of an extreme dietary specialisation, the olfactory system of worm-eating rodents. *Scientific Reports*, 8, 17806.

- Martinez, Q., Okrouhlik, J., Šumbera, R., Wright, M., Araújo, R., Braude, S., Hildebrandt, T. B., Holtze, S., Ruf, I., & Fabre, P.-H. (2023). Mammalian maxilloturbinal evolution does not reflect thermal biology. *Nature Communications*, *14*, 4425.
- Melin, A. D., Veilleux, C. C., Janiak, M. C., Hiramatsu, C., Sánchez-Solano, K. G., Lundeen, I. K., Webb, S. E., Williamson, R. E., Mah, M. A., Murillo-Chacon, E., Schaffner, C. M., Hernández-Salazar, L., Aureli, F., & Kawamura, S. (2022). Anatomy and dietary specialization influence sensory behaviour among sympatric primates. *Proceedings of the Royal Society B: Biological Sciences*, *289*, 20220847.
- Negus, V. (1958). *The comparative anatomy and physiology of the nose and paranasal sinuses*. E. & S. Livingstone.
- Niimura, Y., Matsui, A., & Touhara, K. (2018). Acceleration of olfactory receptor gene loss in primate evolution: Possible link to anatomical change in sensory systems and dietary transition. *Molecular Biology and Evolution*, *35*, 1437–1450.
- Pang, B., Yee, K. K., Lischka, F. W., Rawson, N. E., Haskins, M. E., Wysocki, C. J., Craven, B. A., & Van Valkenburgh, B. (2016). The influence of nasal airflow on respiratory and olfactory epithelial distribution in felids. *Journal of Experimental Biology*, *219*, 1866–1874.
- Parsons, T. S. (1967). Evolution of the nasal structure in the lower tetrapods. *American Zoologist*, *7*, 397–413.
- Paulli, S. (1900a). Über die Pneumaticität des Schädels bei den Säugetieren. Eine morphologische Studie. I. Über den Bau des Siebbeins. Über die Morphologie des Siebbeins und die Pneumaticität bei den Monotremen und den Marsupialiern.
- Paulli, S. (1900b). Über die Pneumaticität des Schädels bei den Säugetieren. Eine morphologische Studie. II. Über die Morphologie des Siebbeins und die Pneumaticität bei den Ungulaten und Probosciden.
- Paulli, S. (1900c). Über die Pneumaticität des Schädels bei den Säugetieren. Eine morphologische Studie. III. Über die Morphologie des Siebbeins und die Pneumaticität bei den Insectivoren, Hyracoideen, Chiropteren, Carnivoren, Pinnipeden, Edentaten, Rodentiern, Prosimiern und Primaten, nebst einer zusammenfassenden Übersicht über die Morphologie des Siebbeins und die der Pneumaticität des Schädels bei den Säugetieren.
- Peri, E., Gingerich, P. D., Aringhieri, G., & Bianucci, G. (2020). Reduction of olfactory and respiratory turbinates in the transition of whales from land to sea: The semiaquatic middle Eocene *Aegyptocetus tarfa*. *Journal of Anatomy*, *236*, 98–104.
- Redford, K. H. (1986). Dietary specialization and variation in two mammalian myrmecophages (variation in mammalian myrmecophagy). *Revista Chilena de Historia Natural*, *59*(1), 201–208.
- Rowe, T. B., Eiting, T. P., Macrini, T. E., & Ketcham, R. A. (2005). Organization of the olfactory and respiratory skeleton in the nose of the gray short-tailed opossum *Monodelphis domestica*. *Journal of Mammalian Evolution*, *12*, 303–336.
- Ruf, I. (2014). Comparative anatomy and systematic implications of the turbinal skeleton in Lagomorpha (Mammalia). *The Anatomical Record*, *297*, 2031–2046.
- Ruf, I. (2020). Ontogenetic transformations of the ethmoidal region in Muroidea (Rodentia, Mammalia): New insights from perinatal stages. *Vertebrate Zoology*, *70*, 383–415.
- Rusu, M. C., Săndulescu, M., Mogoantă, C. A., & Jianu, A. M. (2019). The extremely rare concha of Zuckerkandl reviewed and reported. *Romanian Journal of Morphology and Embryology*, *60*, 775–779.
- Schmidt-Nielsen, K., Hainsworth, F. R., & Murrish, D. E. (1970). Counter-current heat exchange in the respiratory passages: Effect on water and heat balance. *Respiration Physiology*, *9*, 263–276.
- Smith, T., & Rossie, J. (2006). Primate olfaction: Anatomy and evolution. In *Olfaction and the brain: Window to the mind* (pp. 135–166). Cambridge University Press.
- Smith, T. D., Bhatnagar, K. P., Rossie, J. B., Docherty, B. A., Burrows, A. M., Cooper, G. M., Mooney, M. p., & Siegel, M. I. (2007). Scaling of the first ethmoturbinal in nocturnal strepsirrhines: Olfactory and respiratory surfaces. *The Anatomical Record*, *290*, 215–237.
- Smith, T. D., Bhatnagar, K. P., Tuladhar, P., & Burrows, A. M. (2004). Distribution of olfactory epithelium in the primate nasal cavity: Are microsmia and macrosmia valid morphological concepts? *The Anatomical Record Part A: Discoveries in Molecular, Cellular, and Evolutionary Biology*, *281A*, 1173–1181.
- Smith, T. D., & Bonar, C. J. (2022). The nasal cavity in agoutis (*Dasyprocta* spp.): A micro-computed tomographic and histological study. *Vertebrate Zoology*, *72*, 95–113.
- Smith, T. D., Corbin, H. M., King, S. E. E., Bhatnagar, K. P., & DeLeon, V. B. (2021). A comparison of diceCT and histology for determination of nasal epithelial type. *PeerJ*, *9*, e12261.
- Smith, T. D., Craven, B. A., Engel, S. M., Van Valkenburgh, B., & DeLeon, V. B. (2021). “Mucosal maps” of the canine nasal cavity: Micro-computed tomography and histology. *The Anatomical Record*, *304*, 127–138.
- Smith, T. D., DeLeon, V. B., Eiting, T. P., Corbin, H. M., Bhatnagar, K. P., & Santana, S. E. (2022). Venous networks in the upper airways of bats: A histological and diceCT study. *The Anatomical Record*, *305*, 1871–1891.
- Smith, T. D., Eiting, T. P., & Bhatnagar, K. P. (2012). A quantitative study of olfactory, non-olfactory, and vomeronasal epithelia in the nasal fossa of the bat *Megaderma lyra*. *Journal of Mammalian Evolution*, *19*, 27–41.
- Smith, T. D., Eiting, T. P., Bonar, C. J., & Craven, B. A. (2014). Nasal morphometry in marmosets: Loss and redistribution of olfactory surface area. *The Anatomical Record*, *297*, 2093–2104.
- Smith, T. D., Martell, M. C., Rossie, J. B., Bonar, C. J., & DeLeon, V. B. (2016). Ontogeny and microanatomy of the nasal turbinates in Lemuriformes. *The Anatomical Record*, *299*, 1492–1510.
- Smith, T. D., & Rossie, J. B. (2008). Nasal fossa of mouse and dwarf lemurs (Primates, Cheirogaleidae). *The Anatomical Record*, *291*, 895–915.
- Smith, T. D., Rossie, J. B., & Bhatnagar, K. P. (2007). Evolution of the nose and nasal skeleton in primates. *Evolutionary Anthropology: Issues, News, and Reviews*, *16*, 132–146.
- Smith, T. D., Ruf, I., & DeLeon, V. B. (2023). Ontogenetic transformation of the cartilaginous nasal capsule in mammals, a review with new observations on bats. *The Anatomical Record*, 1–17. <https://doi.org/10.1002/ar.25152>
- Starck, D. (1960). Das Cranium eines Schimpansenfetus (Pan troglodytes, Blumenbach 1799) von 71 mm Scheitel-Steiß-Laenge, nebst Bemerkungen über die Körperform von Schimpansenfeten. *Morph Jahrb*, *100*, 559–647.

- Stoddart, D. M. (1980). *The ecology of vertebrate olfaction*. Chapman & Hall.
- Storan, M. J., & Key, B. (2006). Septal organ of Grüneberg is part of the olfactory system. *Journal of Comparative Neurology*, 494, 834–844.
- Taylor, W. A., Lindsey, P. A., & Skinner, J. D. (2002). The feeding ecology of the armadillo *Oryzomys azer*. *Journal of Arid Environments*, 50, 135–152.
- Upham, N. S., Esselstyn, J. A., & Jetz, W. (2019). Inferring the mammal tree: Species-level sets of phylogenies for questions in ecology, evolution, and conservation. *PLOS Biology*, 17, e3000494.
- Van Valkenburgh, B., Curtis, A., Samuels, J. X., Bird, D., Fulkerson, B., Meachen-Samuels, J., & Slater, G. J. (2011). Aquatic adaptations in the nose of carnivores: Evidence from the turbinates. *Journal of Anatomy*, 218, 298–310.
- Van Valkenburgh, B., Pang, B., Bird, D., Curtis, A., Yee, K., Wysocki, C., & Craven, B. A. (2014). Respiratory and olfactory turbinates in Feliform and Caniform carnivores: The influence of snout length. *The Anatomical Record*, 297, 2065–2079.
- Voit, M. (1909). Das Primordialcranium des Kaninchens: Unter Berücksichtigung der Deckknochen. *Anatomische Hefte*, 38, 425–616.
- Wagner, F., & Ruf, I. (2019). Who nose the borzoi? Turbinal skeleton in a dolichocephalic dog breed (*Canis lupus familiaris*). *Mammalian Biology*, 94, 106–119.
- Wagner, F., & Ruf, I. (2021). “Forever young”—Postnatal growth inhibition of the turbinal skeleton in brachycephalic dog breeds (*Canis lupus familiaris*). *The Anatomical Record*, 304, 154–189.
- Wilson, D. A., & Sullivan, R. M. (2011). Cortical processing of odor objects. *Neuron*, 72, 506–519.
- Woehrmann-Repenning, A., & Meinel, W. (1977). A comparative study on the nasal fossae of *Tupaia glis* and four insectivores. *Anatomischer Anzeiger*, 142, 331–345.
- Yee, K. K., Craven, B. A., Wysocki, C. J., & Van Valkenburgh, B. (2016). Comparative morphology and histology of the nasal fossa in four mammals: Gray squirrel, bobcat, coyote, and white-tailed deer. *The Anatomical Record*, 299, 840–852.
- Yohe, L. R., Fabbri, M., Lee, D., Davies, K. T. J., Yohe, T. P., Sánchez, M. K. R., Rengifo, E. M., Hall, R., Mutumi, G., Hedrick, B. P., Sadier, A., Simmons, N. B., Sears, K. E., Elizabeth, D., Rossiter, S. J., Bullar, B.-A. S., & Dávalos, L. M. (2022). Ecological constraints on highly evolvable olfactory receptor genes and morphology in neotropical bats. *Evolution*, 76, 2347–2360.

SUPPORTING INFORMATION

Additional supporting information can be found online in the Supporting Information section at the end of this article.

How to cite this article: Martinez, Q., Wright, M., Dubourguier, B., Ito, K., van de Kamp, T., Hamann, E., Zuber, M., Ferreira, G., Blanc, R., Fabre, P.-H., Hautier, L., & Amson, E. (2024). Disparity of turbinal bones in placental mammals. *The Anatomical Record*, 1–29. <https://doi.org/10.1002/ar.25552>